Available at www.ComputerScienceWeb.com
POWERED BY SCIENCE DIRECT®

Signal Processing 83 (2003) 2641–2673

SIGNAL PROCESSING

www.elsevier.com/locate/sigpro

Design of far-field and near-field broadband beamformers using eigenfilters☆

Simon Doclo*, Marc Moonen

Katholieke Universiteit Leuven, Department of Electrical Engineering (ESAT-SCD), Kasteelpark Arenberg 10, B-3001 Heverlee (Leuven), Belgium

Received 16 January 2003; received in revised form 4 July 2003

Abstract

This paper discusses two novel non-iterative design procedures based on eigenfilters for designing broadband beamformers with an arbitrary spatial directivity pattern for an arbitrary microphone configuration. In the conventional eigenfilter technique a reference frequency-angle point is required, whereas in the eigenfilter technique based on a TLS (total least squares) error criterion, no reference point is required. It is shown how to design broadband beamformers in the far-field, near-field and mixed near-field far-field of the microphone array. Both eigenfilter techniques are compared with other broadband beamformer design procedures (least-squares, maximum energy array, non-linear criterion). It will be shown by simulations that among the considered non-iterative design procedures the TLS eigenfilter technique has the best performance, i.e. best resembling the performance of the non-linear design procedure but having a significantly lower computational complexity.

PACS: 43.60.Gk; 43.72.Ew; 43.72.Kb

Keywords: Broadband beamformer; Eigenfilter; TLS error; Far-field; Near-field

1. Introduction

In many speech communication applications, such as hands-free mobile telephony, hearing aids and voice-controlled systems, the recorded microphone signals are corrupted by acoustic background noise and reverberation. Background noise and reverberation cause a signal degradation which can lead to total unintelligibility of the speech and which decreases the performance of speech recognition and coding systems. Therefore efficient signal enhancement algorithms are required.

☆ This research was supported by the F.W.O. Research Project G.0233.01, the IWT Projects 020540 and 020476, the Concerted Research Action GOA-MEFISTO-666 of the Flemish Government, the Interuniversity Attraction Pole IUAP P5-22 and was partially sponsored by Cochlear.

* Corresponding author. Tel.: +32-16-321899; fax: +32-16-321970.
E-mail addresses: simon.doclo@esat.kuleuven.ac.be (S. Doclo), marc.moonen@esat.kuleuven.ac.be (M. Moonen).

0165-1684/$ - see front matter © 2003 Elsevier B.V. All rights reserved.
doi:10.1016/j.sigpro.2003.07.005

Nomenclature

N	number of microphones
L	length of the FIR filter $\mathbf{w}_n$
M	dimension of the stacked filter vector $\mathbf{w}$ ($M = LN$)
K	number of linear constraints
c	speed of sound ($c = 340$ m/s)
f_s	sampling frequency
r	distance of the speech source to the centre of the microphone array
ω	normalised frequency
θ	angle
d_n	distance between the nth microphone and the centre of the microphone array
$a_n(\theta, r)$	attenuation for the nth microphone
$\tau_n(\theta), \tau_n(\theta, r)$	delay for the nth microphone
$D(\omega, \theta), D(\omega, \theta, r)$	desired spatial directivity pattern
$F(\omega, \theta), F(\omega, \theta, r)$	weighting function
$H(\omega, \theta), H(\omega, \theta, r)$	spatial directivity pattern
$Y_n(\omega, \theta), Y_n(\omega, \theta, r)$	nth microphone signal
$\mathbf{g}(\omega, \theta), \mathbf{g}(\omega, \theta, r)$	steering vector
$\mathbf{G}(\omega, \theta), \mathbf{G}(\omega, \theta, r)$	steering matrix
$\mathbf{w}_n$	filter on the nth microphone
$\mathbf{w}$	stacked filter vector
$\mathbf{C}, \mathbf{b}$	linear constraint matrix/vector
$\mathbf{I}_L$	$L \times L$-dimensional identity matrix
$\mathbf{J}_L$	$L \times L$-dimensional reverse identity matrix

Well-known multi-microphone signal enhancement techniques are fixed and adaptive beamforming [36], which have already been successfully applied in hands-free communication [9] and hearing aids [14,19]. Fixed beamformers (with a fixed spatial directivity pattern) try to obtain spatial focusing on the speech source, thereby reducing reverberation and suppressing background noise not coming from the same direction as the speech source. In general, fixed beamformers have the advantage of having a low computational complexity, not requiring a control algorithm and being more robust than adaptive beamformers, although they are not able to adapt to changing acoustic environments and therefore usually have a lower noise reduction performance. Nevertheless, fixed beamformers are frequently used in highly reverberant environments, in applications where the position of the speech source is assumed to be known (e.g. hearing aids [18,32,33] and car applications) and for creating multiple beams [20,35]. Furthermore, fixed beamformers are used for creating the speech and the noise reference signals in a generalised sidelobe canceller (GSC) [13,15,16], a well-known adaptive beamforming technique. In a GSC it is very important that the fixed beamformers have the desired frequency and spatial filtering behaviour, in order to limit signal leakage into the noise references and hence signal distortion and signal cancellation [28].

This paper discusses the design of far-field and near-field *broadband* beamformers with a given *arbitrary spatial directivity pattern* for a given *arbitrary microphone array configuration*, using an FIR *filter-and-sum* beamformer structure. In speech communication applications, broadband design implies a design over several octaves (e.g. 300–3500 Hz with sampling frequency $f_s = 8$ kHz). Using well-known types of fixed beamformers, such as delay-and-sum beamforming, weighted-sum beamforming [8], differential microphone

arrays [10], superdirective microphone arrays [2,6,18] and frequency-invariant beamforming [38,39], it is not possible to design arbitrary spatial directivity patterns for arbitrary microphone array configurations. For example, differential microphones require a small-size microphone array, superdirective microphone arrays are designed using an assumption about the noise field, and for frequency-invariant beamformers the desired spatial directivity pattern is equal for all frequencies.

For designing broadband beamformers with an arbitrary spatial directivity pattern, several design procedures exist, which are e.g. based on least-squares (LS) filter design [25], a maximum energy array [22] or non-linear optimisation techniques [17,23,24,27]. Although in general we would like to use the non-linear design procedure, this procedure gives rise to a high computational complexity, since it requires an iterative optimisation technique. In this paper two novel non-iterative design procedures are presented, which are based on eigenfilters. In the conventional eigenfilter technique, a reference point is required, whereas in the eigenfilter technique based on a TLS error criterion, no reference point is required. Eigenfilters have already been used for designing 1-D linear-phase FIR filters [30,34] and for designing 2-D and spatial filters [4,29,30]. In this paper we extend their usage to the design of far-field, near-field and mixed near-field far-field broadband beamformers. It will be shown by simulations that the TLS eigenfilter technique has a better performance than the LS, the maximum energy array and the conventional eigenfilter technique.

Many broadband beamformer design procedures either perform the design individually for separate frequencies or approximate the double integrals that arise in the design by a finite sum over a grid of frequencies and angles. However, in this paper we will always calculate such integrals exactly over the frequency-angle plane and hence perform a true broadband design.

When the speech source is close to the microphone array, it is said to be in the near-field and the far-field assumptions are no longer valid [26]. Superdirective and frequency-invariant beamformers, e.g. have been designed for the near-field case in [21,31]. In this paper we will discuss the design of near-field broadband beamformers with an arbitrary spatial directivity pattern, and beamformers that operate both in the near-field and the far-field of the microphone array. It will be shown that for near-field design and for mixed near-field far-field design, the same cost functions as for the far-field case can be used.

This paper is organised as follows. In Section 2 the far-field broadband beamforming problem is introduced and some definitions and notational conventions are given. Section 3 discusses several cost functions that can be used for designing far-field and near-field broadband beamformers. In general, we would like to use the non-linear cost function, minimising the error between the amplitudes of the actual and the desired spatial directivity pattern. However, for this cost function no closed-form solution is available and an iterative non-linear optimisation procedure is required, giving rise to a high computational complexity. Hence, we will also consider other cost functions with a lower computational complexity that can be solved using non-iterative optimisation techniques, such as the least-squares and the maximum energy array cost function. For all cost functions, it will be shown how linear constraints can be imposed on the filter coefficients. Section 4 describes two novel non-iterative eigenfilter-based procedures for designing broadband beamformers. In Section 4.1 the conventional eigenfilter (with reference point) is discussed, whereas Section 4.2 discusses the eigenfilter based on a TLS error criterion. It is shown how both cost functions can be optimised with/without imposing linear constraints. Section 5 discusses the design of near-field broadband beamformers for a predefined distance from the microphone array. It is shown that the same design procedures and cost functions as for the far-field case can be used; the only difference lies in the calculation of the double integrals involved. This section also discusses design procedures for broadband beamformers that operate at several distances. Although this extension is straightforward for most cost functions, for the TLS eigenfilter and for the maximum energy array cost function this extension leads to a significantly different optimisation problem, for which no closed-form solution is available. Section 6 discusses simulation results for the different cost functions and design cases. It is shown that among the considered non-iterative design procedures the TLS eigenfilter technique has the best performance, i.e. best resembling the performance of the non-linear design procedure but having a significantly

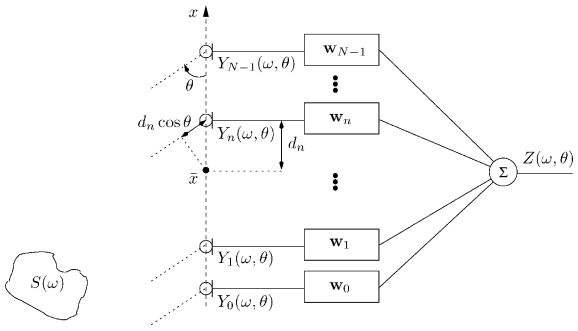

Fig. 1. Linear microphone array configuration (far-field).

lower computational complexity and that mixed near-field far-field design provides a trade-off between the near-field and the far-field performance.

2. Far-field broadband beamforming: configuration

Consider the linear microphone array depicted in Fig. 1, with N microphones and d_n the distance between the nth microphone and the centre of the microphone array. The *spatial directivity pattern* $H(\omega,\theta)$ for a source $S(\omega)$ with normalised frequency ω at an angle θ from the microphone array is defined as

$$H(\omega,\theta)=\frac{Z(\omega,\theta)}{\bar{Y}(\omega,\theta)}=\frac{\sum_{n=0}^{N-1} W_n(\omega)Y_n(\omega,\theta)}{\bar{Y}(\omega,\theta)}, \tag{1}$$

with $\bar{Y}(\omega,\theta)$ the signal received at the centre of the microphone array and $W_n(\omega)$ the frequency response of the real-valued L-dimensional FIR filter $\mathbf{w}_n$,

$$W_n(\omega)=\sum_{l=0}^{L-1} w_{n,l}\mathrm{e}^{-\mathrm{j}l\omega}=\mathbf{w}_n^{\mathrm{T}}\mathbf{e}(\omega), \tag{2}$$

with

$$\mathbf{w}_n=\begin{bmatrix} w_{n,0}\\ w_{n,1}\\ \vdots\\ w_{n,L-1}\end{bmatrix},\quad \mathbf{e}(\omega)=\begin{bmatrix} 1\\ \mathrm{e}^{-\mathrm{j}\omega}\\ \vdots\\ \mathrm{e}^{-\mathrm{j}(L-1)\omega}\end{bmatrix}. \tag{3}$$

When the signal source is far enough from the microphone array (cf. Section 5), the far-field assumptions are valid, i.e. the wavefronts can be assumed to be planar and all microphone signals can be assumed to be equally attenuated. The microphone signals $Y_n(\omega,\theta)$, $n=0\ldots N-1$, then differ by a phase factor from the signal $\bar{Y}(\omega,\theta)$, i.e. $Y_n(\omega,\theta)=\bar{Y}(\omega,\theta)\mathrm{e}^{-\mathrm{j}\omega\tau_n(\theta)}$, $-\pi\leqslant\omega\leqslant\pi$, $-\pi\leqslant\theta\leqslant\pi$, with the delay $\tau_n(\theta)$ in number of samples equal to

$$\tau_n(\theta)=\frac{d_n\cos\theta}{c}f_s, \tag{4}$$

with c the speed of sound ($c = 340$ m/s) and f_s the sampling frequency. Combining (1) and (4), the spatial directivity pattern $H(\omega,\theta)$ can be written as

$$\boxed{H(\omega,\theta) = \sum_{n=0}^{N-1} W_n(\omega) e^{-j\omega\tau_n(\theta)} = \sum_{n=0}^{N-1} \mathbf{w}_n^T \mathbf{e}(\omega) e^{-j\omega\tau_n(\theta)} = \mathbf{w}^T \mathbf{g}(\omega,\theta)} \tag{5}$$

with the M-dimensional stacked filter vector $\mathbf{w}$ and the steering vector $\mathbf{g}(\omega,\theta)$, with $M = LN$, equal to

$$\mathbf{w} = \begin{bmatrix} \mathbf{w}_0 \\ \mathbf{w}_1 \\ \vdots \\ \mathbf{w}_{N-1} \end{bmatrix}, \quad \mathbf{g}(\omega,\theta) = \begin{bmatrix} \mathbf{e}(\omega) e^{-j\omega\tau_0(\theta)} \\ \mathbf{e}(\omega) e^{-j\omega\tau_1(\theta)} \\ \vdots \\ \mathbf{e}(\omega) e^{-j\omega\tau_{N-1}(\theta)} \end{bmatrix}. \tag{6}$$

The steering vector $\mathbf{g}(\omega,\theta)$ can be decomposed into a real and an imaginary part, $\mathbf{g}(\omega,\theta) = \mathbf{g}_R(\omega,\theta) + j\mathbf{g}_I(\omega,\theta)$. The ith element of $\mathbf{g}_R(\omega,\theta)$ is equal to

$$\mathbf{g}_R^i(\omega,\theta) = \cos\left[\omega\left(k + \frac{d_n \cos\theta}{c} f_s\right)\right], \quad i = 1 \ldots M, \tag{7}$$

with $k = \mathrm{mod}(i-1, L)$ and $n = \lfloor (i-1)/L \rfloor$, where $\lfloor (i-1)/L \rfloor$ denotes the largest integer smaller than or equal to $(i-1)/L$, and $\mathrm{mod}(i-1, L)$ is the remainder of the division.

Using (5), the spatial directivity spectrum $|H(\omega,\theta)|^2$ can be written as

$$|H(\omega,\theta)|^2 = H(\omega,\theta) H^*(\omega,\theta) = \mathbf{w}^T \mathbf{G}(\omega,\theta) \mathbf{w}, \tag{8}$$

with $\mathbf{G}(\omega,\theta) = \mathbf{g}(\omega,\theta)\mathbf{g}^H(\omega,\theta)$. The steering matrix $\mathbf{G}(\omega,\theta)$ can be decomposed into a real and an imaginary part, $\mathbf{G}(\omega,\theta) = \mathbf{G}_R(\omega,\theta) + j\mathbf{G}_I(\omega,\theta)$. Since $\mathbf{G}_I(\omega,\theta)$ is anti-symmetric, the spatial directivity spectrum $|H(\omega,\theta)|^2$ is equal to

$$\boxed{|H(\omega,\theta)|^2 = \mathbf{w}^T \mathbf{G}_R(\omega,\theta) \mathbf{w}}. \tag{9}$$

The (i,j)th element of the real part $\mathbf{G}_R(\omega,\theta)$ is equal to

$$\mathbf{G}_R^{ij}(\omega,\theta) = \cos\left[\omega\left((k-l) + \frac{(d_n - d_m)\cos\theta}{c} f_s\right)\right], \tag{10}$$

with $k = \mathrm{mod}(i-1, L)$, $l = \mathrm{mod}(j-1, L)$, $n = \lfloor (i-1)/L \rfloor$ and $m = \lfloor (j-1)/L \rfloor$.

3. Broadband beamforming procedures

3.1. Overview

The design of a broadband beamformer consists of the calculation of the filter $\mathbf{w}$, such that $H(\omega,\theta)$ optimally fits a desired spatial directivity pattern $D(\omega,\theta)$, where $D(\omega,\theta)$ is an arbitrary two-dimensional function in ω and θ. Several design procedures exist, depending on the specific cost function which is optimised. In this

section three different cost functions will be considered:

- a least-squares (LS) cost function J_{LS}, minimising the least-squares error between the actual and the desired spatial directivity pattern, which can be written as a quadratic function (cf. Section 3.2);
- a maximum energy array cost function J_{ME}, maximising the energy ratio between the passband and the stopband region. Maximising this cost function leads to a generalised eigenvalue problem (cf. Section 3.3);
- a non-linear cost function J_{NL}, minimising the error between the amplitudes of the actual and the desired spatial directivity pattern, not taking into account the phase of the spatial directivity patterns. Minimising this cost function leads to a non-linear optimisation problem, which needs to be solved using iterative optimisation techniques (cf. Section 3.4).

In general we would like to use the non-linear cost function J_{NL}. However, since optimising this cost function requires an iterative non-linear optimisation technique (cf. Section 3.4.3), giving rise to a large computational complexity, we will also consider non-iterative design procedures (least-squares, maximum energy array) with a lower computational complexity. In addition, in Section 4 two non-iterative eigenfilter-based cost functions will be defined and in Section 6 the performance of all considered non-iterative design procedures will be compared with the non-linear design procedure.

We will consider the design of broadband beamformers over the total frequency-angle plane of interest, i.e. we will not split up the fullband problem into separate smallband problems for different frequencies. Moreover, we will not approximate the double integrals over the frequency-angle plane by a finite Riemann-sum over a grid of frequencies and angles, as e.g has been done in [17] for the non-linear cost function. For all cost functions, we will first discuss the general design procedure for an arbitrary function $D(\omega,\theta)$, and we will then focus on the specific design case of a broadband beamformer having a desired response $D(\omega,\theta)=0$ in the stopband region $(\Omega_{\mathrm{s}},\Theta_{\mathrm{s}})$ and $D(\omega,\theta)=1$ in the passband region $(\Omega_{\mathrm{p}},\Theta_{\mathrm{p}})$. For the specific design case, the weighting function $F(\omega,\theta)=1$ in the passband and $F(\omega,\theta)=\alpha$ in the stopband. We will also discuss how linear constraints of the form $\mathbf{Cw}=\mathbf{b}$ can be imposed on the filter $\mathbf{w}$ (cf. Section 3.5).

3.2. Least-squares design procedure

The least-squares (LS) cost function is a well-known cost function from literature, which can for example be used for designing FIR filters [25], 2D-filters [29] and broadband beamformers.

3.2.1. General design

Considering the LS error $|H(\omega,\theta)-D(\omega,\theta)|^2$, the LS cost function is defined as

$$J_{\mathrm{LS}}(\mathbf{w})=\int_{\Theta}\int_{\Omega}F(\omega,\theta)|H(\omega,\theta)-D(\omega,\theta)|^2\,\mathrm{d}\omega\,\mathrm{d}\theta, \tag{11}$$

where both the phase and the amplitude of $H(\omega,\theta)$ are taken into account. $F(\omega,\theta)$ is a positive real weighting function, assigning more or less importance to certain frequencies or angles. Using $F(\omega,\theta)$ it is for example possible to use a speech-intelligibility motivated frequency weighting [1]. The LS cost function can be written as

$$\begin{aligned}J_{\mathrm{LS}}(\mathbf{w})=&\int_{\Theta}\int_{\Omega}F(\omega,\theta)|H(\omega,\theta)|^2\,\mathrm{d}\omega\,\mathrm{d}\theta+\int_{\Theta}\int_{\Omega}F(\omega,\theta)|D(\omega,\theta)|^2\,\mathrm{d}\omega\,\mathrm{d}\theta\\&-2\int_{\Theta}\int_{\Omega}F(\omega,\theta)\mathrm{Re}\{D(\omega,\theta)H^*(\omega,\theta)\}.\end{aligned} \tag{12}$$

Using (9) and the fact that

$$\mathrm{Re}\{D(\omega,\theta)H^*(\omega,\theta)\} = \mathbf{w}^{\mathrm{T}}[D_{\mathrm{R}}(\omega,\theta)\mathbf{g}_{\mathrm{R}}(\omega,\theta) + D_{\mathrm{I}}(\omega,\theta)\mathbf{g}_{\mathrm{I}}(\omega,\theta)], \tag{13}$$

this cost function can be rewritten as the quadratic function

$$\boxed{J_{\mathrm{LS}}(\mathbf{w}) = \mathbf{w}^{\mathrm{T}}\mathbf{Q}_{\mathrm{LS}}\mathbf{w} - 2\mathbf{w}^{\mathrm{T}}\mathbf{a} + d_{\mathrm{LS}}} \tag{14}$$

with

$$\mathbf{Q}_{\mathrm{LS}} = \int_{\Theta}\int_{\Omega} F(\omega,\theta)\mathbf{G}_{\mathrm{R}}(\omega,\theta)\,\mathrm{d}\omega\,\mathrm{d}\theta, \tag{15}$$

$$\mathbf{a} = \int_{\Theta}\int_{\Omega} F(\omega,\theta)[D_{\mathrm{R}}(\omega,\theta)\mathbf{g}_{\mathrm{R}}(\omega,\theta) + D_{\mathrm{I}}(\omega,\theta)\mathbf{g}_{\mathrm{I}}(\omega,\theta)]\,\mathrm{d}\omega\,\mathrm{d}\theta, \tag{16}$$

$$d_{\mathrm{LS}} = \int_{\Theta}\int_{\Omega} F(\omega,\theta)|D(\omega,\theta)|^2\,\mathrm{d}\omega\,\mathrm{d}\theta. \tag{17}$$

The LS cost function $J_{\mathrm{LS}}(\mathbf{w})$ is minimised by setting the derivative $\partial J_{\mathrm{LS}}(\mathbf{w})/\partial\mathbf{w}$ equal to 0, such that the solution $\mathbf{w}_{\mathrm{LS}}$ is given by

$$\boxed{\mathbf{w}_{\mathrm{LS}} = \mathbf{Q}_{\mathrm{LS}}^{-1}\mathbf{a}}. \tag{18}$$

3.2.2. Specific design case

For the specific design case where $D(\omega,\theta) = 1$ and $F(\omega,\theta) = 1$ in the passband and $D(\omega,\theta) = 0$ and $F(\omega,\theta) = \alpha$ in the stopband, Eqs. (15)–(17) can be written as

$$\mathbf{Q}_{\mathrm{LS}} = \underbrace{\int_{\Theta_{\mathrm{p}}}\int_{\Omega_{\mathrm{p}}} \mathbf{G}_{\mathrm{R}}(\omega,\theta)\,\mathrm{d}\omega\,\mathrm{d}\theta}_{\mathbf{Q}_{\mathrm{e}}^{\mathrm{p}}} + \underbrace{\alpha\int_{\Theta_{\mathrm{s}}}\int_{\Omega_{\mathrm{s}}} \mathbf{G}_{\mathrm{R}}(\omega,\theta)\,\mathrm{d}\omega\,\mathrm{d}\theta}_{\mathbf{Q}_{\mathrm{e}}^{\mathrm{s}}}, \tag{19}$$

$$\mathbf{a} = \int_{\Theta_{\mathrm{p}}}\int_{\Omega_{\mathrm{p}}} \mathbf{g}_{\mathrm{R}}(\omega,\theta)\,\mathrm{d}\omega\,\mathrm{d}\theta, \qquad d_{\mathrm{LS}} = \int_{\Theta_{\mathrm{p}}}\int_{\Omega_{\mathrm{p}}} 1\,\mathrm{d}\omega\,\mathrm{d}\theta. \tag{20}$$

The quantity $\mathbf{w}^{\mathrm{T}}\mathbf{Q}_{\mathrm{e}}^{\mathrm{p}}\mathbf{w}$ is equal to the energy in the passband, whereas $\mathbf{w}^{\mathrm{T}}\mathbf{Q}_{\mathrm{e}}^{\mathrm{s}}\mathbf{w}$ is equal to the energy in the stopband. Using (7) and (10), the ith element of $\mathbf{a}$ and the (i,j)th element of $\mathbf{Q}_{\mathrm{e}}$ (i.e. $\mathbf{Q}_{\mathrm{e}}^{\mathrm{p}}$ or $\mathbf{Q}_{\mathrm{e}}^{\mathrm{s}}$) are equal to

$$\mathbf{a}^i = \int_{\Theta_{\mathrm{p}}}\int_{\Omega_{\mathrm{p}}} \mathbf{g}_{\mathrm{R}}^i(\omega,\theta)\,\mathrm{d}\omega\,\mathrm{d}\theta = \int_{\Theta_{\mathrm{p}}}\int_{\Omega_{\mathrm{p}}} \cos\left[\omega\left(k + \frac{d_n\cos\theta}{c}f_{\mathrm{s}}\right)\right]\mathrm{d}\omega\,\mathrm{d}\theta,$$

$$\mathbf{Q}_{\mathrm{e}}^{ij} = \int_{\Theta}\int_{\Omega} \mathbf{G}_{\mathrm{R}}^{ij}(\omega,\theta)\,\mathrm{d}\omega\,\mathrm{d}\theta = \int_{\Theta}\int_{\Omega} \cos\left[\omega\left((k-l) + \frac{(d_n - d_m)\cos\theta}{c}f_{\mathrm{s}}\right)\right]\mathrm{d}\omega\,\mathrm{d}\theta, \tag{21}$$

with $k=\mathrm{mod}(i-1,L)$, $l=\mathrm{mod}(j-1,L)$, $n=\lfloor (i-1)/L \rfloor$ and $m=\lfloor (j-1)/L \rfloor$. These integrals can be considered to be special cases of the integral

$$\int_{\theta_1}^{\theta_2} \int_{\omega_1}^{\omega_2} \cos[\omega(\alpha+\beta\cos\theta)+\gamma]\,\mathrm{d}\omega\,\mathrm{d}\theta, \tag{22}$$

of which the computation is discussed in Appendix A.

3.2.3. Linear constraints

Different linear constraints of the form $\mathbf{C}\mathbf{w}=\mathbf{b}$, with $\mathbf{C}$ a $K\times M$-dimensional matrix and $\mathbf{b}$ a K-dimensional vector, will be discussed in Section 3.5. When imposing linear constraints on the LS criterion, the constrained optimisation problem has the form

$$\boxed{\min_{\mathbf{w}} \mathbf{w}^{\mathrm{T}}\mathbf{Q}_{\mathrm{LS}}\mathbf{w} - 2\mathbf{w}^{\mathrm{T}}\mathbf{a} + d_{\mathrm{LS}} \quad \text{subject to } \mathbf{C}\mathbf{w}=\mathbf{b}}. \tag{23}$$

This constrained minimisation problem can be transformed into an unconstrained minimisation problem (similar to the derivation of the Generalised Sidelobe Canceller [3,13]) and the solution $\mathbf{w}_{\mathrm{LS}}^{\mathrm{c}}$ of the constrained minimisation problem is equal to

$$\boxed{\mathbf{w}_{\mathrm{LS}}^{\mathrm{c}} = \mathbf{Q}_{\mathrm{LS}}^{-1}\mathbf{C}^{\mathrm{T}}(\mathbf{C}\mathbf{Q}_{\mathrm{LS}}^{-1}\mathbf{C}^{\mathrm{T}})^{-1}(\mathbf{b}-\mathbf{C}\mathbf{Q}_{\mathrm{LS}}^{-1}\mathbf{a}) + \mathbf{Q}_{\mathrm{LS}}^{-1}\mathbf{a}}. \tag{24}$$

3.3. Maximum energy array

In [22] a so-called maximum energy array cost function has been defined. Since in the design of a maximum energy array broadband beamformer it is assumed that a passband region and a stopband region are present, we can only consider the specific design case for the maximum energy array cost function.

3.3.1. Specific design case

The maximum energy array cost function $J_{\mathrm{ME}}(\mathbf{w})$ is defined as the ratio of the energy in one frequency-angle region (passband) and the energy in another frequency-angle region (stopband), i.e.

$$J_{\mathrm{ME}}(\mathbf{w}) = \frac{\int_{\Theta_{\mathrm{p}}}\int_{\Omega_{\mathrm{p}}} |H(\omega,\theta)|^2\,\mathrm{d}\omega\,\mathrm{d}\theta}{\int_{\Theta_{\mathrm{s}}}\int_{\Omega_{\mathrm{s}}} |H(\omega,\theta)|^2\,\mathrm{d}\omega\,\mathrm{d}\theta}. \tag{25}$$

Maximising this ratio can actually be considered as a broadband generalisation of the (smallband) superdirective beamformer formulation [2]. Using (19), this cost function can be written as

$$\boxed{J_{\mathrm{ME}}(\mathbf{w}) = \frac{\mathbf{w}^{\mathrm{T}}\mathbf{Q}_{\mathrm{c}}^{\mathrm{p}}\mathbf{w}}{\mathbf{w}^{\mathrm{T}}\mathbf{Q}_{\mathrm{c}}^{\mathrm{s}}\mathbf{w}}}. \tag{26}$$

The filter $\mathbf{w}_{\mathrm{ME}}$ which maximises $J_{\mathrm{ME}}(\mathbf{w})$ is equal to the generalised eigenvector corresponding to the maximum generalised eigenvalue in the generalised eigenvalue decomposition (GEVD) of $\mathbf{Q}_{\mathrm{c}}^{\mathrm{p}}$ and $\mathbf{Q}_{\mathrm{c}}^{\mathrm{s}}$. However, as will be shown in the simulations, the spatial directivity pattern corresponding to this filter mainly amplifies the high frequencies, since it is easier to obtain a large directivity for high frequencies than for low frequencies (cf. delay-and-sum beamformer). Hence, a frequency-dependent angle integration interval has to be used with a larger integration interval at low frequencies [22], or alternatively, linear constraints have to be imposed.

3.3.2. Linear constraints

When imposing linear constraints of the form $\mathbf{C}\mathbf{w} = \mathbf{b}$, the constrained optimisation problem can be written as

$$\boxed{\max_{\mathbf{w}} \frac{\mathbf{w}^{\mathrm{T}}\mathbf{Q}_{\mathrm{e}}^{\mathrm{p}}\mathbf{w}}{\mathbf{w}^{\mathrm{T}}\mathbf{Q}_{\mathrm{e}}^{\mathrm{s}}\mathbf{w}} \quad \text{subject to } \mathbf{C}\mathbf{w} = \mathbf{b}} \tag{27}$$

with $\mathbf{b}$ generally not equal to $\mathbf{0}$.[1] This constrained ratio maximisation problem can be rewritten as the extended constrained ratio maximisation problem

$$\max_{\hat{\mathbf{w}}} \frac{\hat{\mathbf{w}}^{\mathrm{T}}\hat{\mathbf{Q}}_{\mathrm{e}}^{\mathrm{p}}\hat{\mathbf{w}}}{\hat{\mathbf{w}}^{\mathrm{T}}\hat{\mathbf{Q}}_{\mathrm{e}}^{\mathrm{s}}\hat{\mathbf{w}}} \quad \text{subject to } \hat{\mathbf{C}}\hat{\mathbf{w}} = \mathbf{0}, \tag{28}$$

with the extended vector $\hat{\mathbf{w}}$ and matrices $\hat{\mathbf{C}}$, $\hat{\mathbf{Q}}_{\mathrm{e}}^{\mathrm{p}}$ and $\hat{\mathbf{Q}}_{\mathrm{e}}^{\mathrm{s}}$ defined as

$$\hat{\mathbf{w}} = \begin{bmatrix} \mathbf{w} \\ -1 \end{bmatrix}, \quad \hat{\mathbf{C}} = [\,\mathbf{C} \quad \mathbf{b}\,], \quad \hat{\mathbf{Q}}_{\mathrm{e}}^{\mathrm{p}} = \begin{bmatrix} \mathbf{Q}_{\mathrm{e}}^{\mathrm{p}} & \mathbf{0} \\ \mathbf{0}^{\mathrm{T}} & 0 \end{bmatrix}, \quad \hat{\mathbf{Q}}_{\mathrm{e}}^{\mathrm{s}} = \begin{bmatrix} \mathbf{Q}_{\mathrm{e}}^{\mathrm{s}} & \mathbf{0} \\ \mathbf{0}^{\mathrm{T}} & 0 \end{bmatrix}. \tag{29}$$

The constrained optimisation problem (28) can be transformed into the unconstrained optimisation problem

$$\max_{\tilde{\mathbf{w}}} \frac{\tilde{\mathbf{w}}^{\mathrm{T}}\mathbf{B}\hat{\mathbf{Q}}_{\mathrm{e}}^{\mathrm{p}}\mathbf{B}^{\mathrm{T}}\tilde{\mathbf{w}}}{\tilde{\mathbf{w}}^{\mathrm{T}}\mathbf{B}\hat{\mathbf{Q}}_{\mathrm{e}}^{\mathrm{s}}\mathbf{B}^{\mathrm{T}}\tilde{\mathbf{w}}}, \tag{30}$$

with $\hat{\mathbf{w}} = \mathbf{B}^{\mathrm{T}}\tilde{\mathbf{w}}$ and $\mathbf{B}$ the $(M+1-K)\times(M+1)$-dimensional null space of $\hat{\mathbf{C}}$ and $\tilde{\mathbf{w}}$ an $(M+1-K)$-dimensional vector. The solution $\tilde{\mathbf{w}}_{\mathrm{ME}}$ of the unconstrained optimisation problem is the generalised eigenvector of $\mathbf{B}\hat{\mathbf{Q}}_{\mathrm{e}}^{\mathrm{p}}\mathbf{B}^{\mathrm{T}}$ and $\mathbf{B}\hat{\mathbf{Q}}_{\mathrm{e}}^{\mathrm{s}}\mathbf{B}^{\mathrm{T}}$, corresponding to the maximum generalised eigenvalue, such that the solution $\hat{\mathbf{w}}_{\mathrm{ME}}^{\mathrm{c}}$ of the constrained optimisation problem is equal to

$$\hat{\mathbf{w}}_{\mathrm{ME}}^{\mathrm{c}} = \mathbf{B}^{\mathrm{T}}\tilde{\mathbf{w}}_{\mathrm{ME}}. \tag{31}$$

After scaling the last element of $\hat{\mathbf{w}}_{\mathrm{ME}}^{\mathrm{c}}$ to -1, the actual solution $\mathbf{w}_{\mathrm{ME}}^{\mathrm{c}}$ of (27) is obtained as the first M elements of $\hat{\mathbf{w}}_{\mathrm{ME}}^{\mathrm{c}}$. The fact that the matrices $\hat{\mathbf{Q}}_{\mathrm{e}}^{\mathrm{p}}$ and $\hat{\mathbf{Q}}_{\mathrm{e}}^{\mathrm{s}}$ are singular does not give rise to problems, since the matrices $\mathbf{B}\hat{\mathbf{Q}}_{\mathrm{e}}^{\mathrm{p}}\mathbf{B}^{\mathrm{T}}$ and $\mathbf{B}\hat{\mathbf{Q}}_{\mathrm{e}}^{\mathrm{s}}\mathbf{B}^{\mathrm{T}}$ are in general not singular.

3.4. Non-linear criterion

Different non-linear cost functions for broadband beamforming have been proposed in literature, leading to a minimax problem [23,27] or requiring iterative optimisation techniques [17,24]. In this section we will slightly modify the non-linear cost function presented in [17], such that the double integrals arising in the optimisation problem only need to be computed once.

3.4.1. General design

Instead of minimising the LS error $|H(\omega,\theta) - D(\omega,\theta)|^2$, it is also possible to minimise the error between the amplitudes $|H(\omega,\theta)| - |D(\omega,\theta)|$, because in general the phase of the spatial directivity pattern is of no relevance. This problem formulation leads to the cost function [17]

$$\bar{J}_{\mathrm{NL}}(\mathbf{w}) = \int_{\Theta}\int_{\Omega} F(\omega,\theta)[|H(\omega,\theta)| - |D(\omega,\theta)|]^2 \,\mathrm{d}\omega\,\mathrm{d}\theta, \tag{32}$$

[1] If $\mathbf{b} = \mathbf{0}$, this optimisation problem reduces to the problem formulation in (28).

which can be rewritten as

$$\bar{J}_{\mathrm{NL}}(\mathbf{w}) = \int_{\Theta}\int_{\Omega} F(\omega,\theta)|H(\omega,\theta)|^2 \,\mathrm{d}\omega\,\mathrm{d}\theta + \int_{\Theta}\int_{\Omega} F(\omega,\theta)|D(\omega,\theta)|^2 \,\mathrm{d}\omega\,\mathrm{d}\theta$$
$$-2\int_{\Theta}\int_{\Omega} F(\omega,\theta)|D(\omega,\theta)||H(\omega,\theta)| \,\mathrm{d}\omega\,\mathrm{d}\theta \tag{33}$$
$$= \mathbf{w}^{\mathrm{T}}\mathbf{Q}_{\mathrm{LS}}\mathbf{w} + d_{\mathrm{LS}} - \underbrace{2\int_{\Theta}\int_{\Omega} F(\omega,\theta)|D(\omega,\theta)||H(\omega,\theta)| \,\mathrm{d}\omega\,\mathrm{d}\theta}_{J_{\mathrm{abs}}(\mathbf{w})}, \tag{34}$$

with $\mathbf{Q}_{\mathrm{LS}}$ and d_{LS} defined respectively in (15) and (17). Minimising $\bar{J}_{\mathrm{NL}}(\mathbf{w})$ leads to a non-linear optimisation problem, which can be solved using iterative optimisation techniques. These optimisation techniques generally involve several evaluations of $\bar{J}_{\mathrm{NL}}(\mathbf{w})$ in each iteration step. A complexity problem now arises in the computation of $J_{\mathrm{abs}}(\mathbf{w})$. Without loss of generality, assume that $F(\omega,\theta)=1$ and $|D(\omega,\theta)|=1$ over some frequency-angle region $(\Theta_{\mathrm{p}},\Omega_{\mathrm{p}})$ and that $D(\omega,\theta)=0$ elsewhere. $J_{\mathrm{abs}}(\mathbf{w})$ can then be written using (9) as

$$J_{\mathrm{abs}}(\mathbf{w}) = 2\int_{\Theta_{\mathrm{p}}}\int_{\Omega_{\mathrm{p}}} |H(\omega,\theta)| \,\mathrm{d}\omega\,\mathrm{d}\theta = 2\int_{\Theta_{\mathrm{p}}}\int_{\Omega_{\mathrm{p}}} \sqrt{\mathbf{w}^{\mathrm{T}}\mathbf{G}_{\mathrm{R}}(\omega,\theta)\mathbf{w}} \,\mathrm{d}\omega\,\mathrm{d}\theta. \tag{35}$$

Because of the square root, the filter coefficients cannot be extracted from the double integral, and *for every* $\mathbf{w}$ *the double integrals need to be recomputed numerically*, which is a computationally very demanding procedure. However, by slightly modifying the non-linear cost function, it is possible to overcome this computational problem.

Instead of minimising the error between the amplitudes $|H(\omega,\theta)|$ and $|D(\omega,\theta)|$, we propose a *novel non-linear criterion* which minimises the error between the square of the amplitudes $|H(\omega,\theta)|^2$ and $|D(\omega,\theta)|^2$, i.e.

$$\boxed{J_{\mathrm{NL}}(\mathbf{w}) = \int_{\Theta}\int_{\Omega} F(\omega,\theta)[|H(\omega,\theta)|^2 - |D(\omega,\theta)|^2]^2 \,\mathrm{d}\omega\,\mathrm{d}\theta} \tag{36}$$

which is also independent of the phase of the spatial directivity patterns. The cost function $J_{\mathrm{NL}}(\mathbf{w})$ can be written (without square-roots) as

$$J_{\mathrm{NL}}(\mathbf{w}) = \int_{\Theta}\int_{\Omega} F(\omega,\theta)(\mathbf{w}^{\mathrm{T}}\mathbf{G}(\omega,\theta)\mathbf{w})^2 \,\mathrm{d}\omega\,\mathrm{d}\theta + \int_{\Theta}\int_{\Omega} F(\omega,\theta)|D(\omega,\theta)|^4 \,\mathrm{d}\omega\,\mathrm{d}\theta$$
$$-2\int_{\Theta}\int_{\Omega} F(\omega,\theta)|D(\omega,\theta)|^2(\mathbf{w}^{\mathrm{T}}\mathbf{G}_{\mathrm{R}}(\omega,\theta)\mathbf{w}) \,\mathrm{d}\omega\,\mathrm{d}\theta \tag{37}$$
$$= J_{\mathrm{sum}}(\mathbf{w}) + d_{\mathrm{NL}} - 2\mathbf{w}^{\mathrm{T}}\mathbf{Q}_{\mathrm{NL}}\mathbf{w}, \tag{38}$$

with

$$J_{\mathrm{sum}}(\mathbf{w}) = \int_{\Theta}\int_{\Omega} F(\omega,\theta)(\mathbf{w}^{\mathrm{T}}\mathbf{G}(\omega,\theta)\mathbf{w})^2 \,\mathrm{d}\omega\,\mathrm{d}\theta \tag{39}$$

$$d_{\mathrm{NL}} = \int_{\Theta}\int_{\Omega} F(\omega,\theta)|D(\omega,\theta)|^4 \,\mathrm{d}\omega\,\mathrm{d}\theta \tag{40}$$

$$\mathbf{Q}_{\mathrm{NL}} = \int_{\Theta}\int_{\Omega} F(\omega,\theta)|D(\omega,\theta)|^2\mathbf{G}_{\mathrm{R}}(\omega,\theta) \,\mathrm{d}\omega\,\mathrm{d}\theta. \tag{41}$$

3.4.2. Specific design case

For the specific design case where $F(\omega,\theta)=1$ and $D(\omega,\theta)=1$ in the passband and $D(\omega,\theta)=0$ and $F(\omega,\theta)=\alpha$ in the stopband, Eqs. (39)–(41) can be written as

$$J_{\mathrm{sum}}(\mathbf{w}) = \underbrace{\int_{\Theta_\mathrm{p}}\int_{\Omega_\mathrm{p}} (\mathbf{w}^\mathrm{T}\mathbf{G}(\omega,\theta)\mathbf{w})^2 \,\mathrm{d}\omega\,\mathrm{d}\theta}_{J^\mathrm{p}_{\mathrm{sum}}(\mathbf{w})} + \alpha \underbrace{\int_{\Theta_\mathrm{s}}\int_{\Omega_\mathrm{s}} (\mathbf{w}^\mathrm{T}\mathbf{G}(\omega,\theta)\mathbf{w})^2 \,\mathrm{d}\omega\,\mathrm{d}\theta}_{J^\mathrm{s}_{\mathrm{sum}}(\mathbf{w})},$$

$$d_{\mathrm{NL}} = \int_{\Theta_\mathrm{p}}\int_{\Omega_\mathrm{p}} 1 \,\mathrm{d}\omega\,\mathrm{d}\theta = d_{\mathrm{LS}} \qquad \mathbf{Q}_{\mathrm{NL}} = \int_{\Theta_\mathrm{p}}\int_{\Omega_\mathrm{p}} \mathbf{G}_\mathrm{R}(\omega,\theta)\,\mathrm{d}\omega\,\mathrm{d}\theta = \mathbf{Q}^\mathrm{p}_\mathrm{e}. \tag{42}$$

Using (8), the expression $|H(\omega,\theta)|^4$, required in the computation of $J_{\mathrm{sum}}(\mathbf{w})$, can be written as

$$|H(\omega,\theta)|^4 = (\mathbf{w}^\mathrm{T}\mathbf{G}(\omega,\theta)\mathbf{w})(\mathbf{w}^\mathrm{T}\mathbf{G}(\omega,\theta)\mathbf{w}) \tag{43}$$

$$= \left(\sum_{i=1}^{M}\sum_{j=1}^{M} w(i)w(j)\mathbf{G}^{ij}(\omega,\theta)\right)\left(\sum_{k=1}^{M}\sum_{l=1}^{M} w(k)w(l)\mathbf{G}^{kl}(\omega,\theta)\right) \tag{44}$$

$$= \sum_{i=1}^{M}\sum_{j=1}^{M}\sum_{k=1}^{M}\sum_{l=1}^{M} w(i)w(j)\,w(k)w(l)\,\mathrm{e}^{-\mathrm{j}\omega(\alpha_{ijkl}+\beta_{ijkl}\cos\theta)}, \tag{45}$$

with

$$\boxed{\alpha_{ijkl} = \mathrm{mod}(i-1,L) - \mathrm{mod}(j-1,L) + \mathrm{mod}(k-1,L) - \mathrm{mod}(l-1,L)}$$

$$\boxed{\beta_{ijkl} = \frac{f_\mathrm{s}}{c}(d_{\lfloor (i-1)/L\rfloor} - d_{\lfloor (j-1)/L\rfloor} + d_{\lfloor (k-1)/L\rfloor} - d_{\lfloor (l-1)/L\rfloor})} \tag{46}$$

Since $|H(\omega,\theta)|^4$ is real (and the filter coefficients are real), only the real part of the exponential function has to be considered, such that

$$|H(\omega,\theta)|^4 = \sum_{i=1}^{M}\sum_{j=1}^{M}\sum_{k=1}^{M}\sum_{l=1}^{M} w(i)w(j)w(k)w(l)\cos[\omega(\alpha_{ijkl}+\beta_{ijkl}\cos\theta)], \tag{47}$$

and $J_{\mathrm{sum}}(\mathbf{w})$ can be written as

$$\boxed{J_{\mathrm{sum}}(\mathbf{w}) = \int_\Theta\int_\Omega |H(\omega,\theta)|^4 \,\mathrm{d}\omega\,\mathrm{d}\theta = \sum_{i=1}^{M}\sum_{j=1}^{M}\sum_{k=1}^{M}\sum_{l=1}^{M} w(i)w(j)w(k)w(l)\rho_{ijkl}} \tag{48}$$

with

$$\rho_{ijkl} = \int_\Theta\int_\Omega \cos[\omega(\alpha_{ijkl}+\beta_{ijkl}\cos\theta)]\,\mathrm{d}\omega\,\mathrm{d}\theta. \tag{49}$$

These integrals are discussed in Appendix A and only need to be computed once (since ρ_{ijkl} is independent of $\mathbf{w}$). Therefore the function $J_{\mathrm{sum}}(\mathbf{w})$, and hence the total cost function $J_{\mathrm{NL}}(\mathbf{w})$, can be evaluated *without having to calculate double integrals for every* $\mathbf{w}$.

3.4.3. Non-linear optimisation technique

Minimising $J_{\mathrm{NL}}(\mathbf{w})$ requires an iterative non-linear optimisation technique, for which we have for example used a medium-scale quasi-Newton method with cubic polynomial line search or a large-scale subspace trust region method [5,12]. In order to improve the numerical robustness and the convergence speed, both the gradient and the Hessian

$$\frac{\partial J_{\mathrm{NL}}(\mathbf{w})}{\partial \mathbf{w}} = \frac{\partial J_{\mathrm{sum}}(\mathbf{w})}{\partial \mathbf{w}} - 4\mathbf{Q}_{\mathrm{NL}}\mathbf{w}, \tag{50}$$

$$\mathbf{H}_{\mathrm{NL}}(\mathbf{w}) = \frac{\partial^2 J_{\mathrm{NL}}(\mathbf{w})}{\partial^2 \mathbf{w}} = \frac{\partial^2 J_{\mathrm{sum}}(\mathbf{w})}{\partial^2 \mathbf{w}} - 4\mathbf{Q}_{\mathrm{NL}}, \tag{51}$$

can be supplied analytically. It can be shown (for details, we refer to [7]) that

$$\boxed{\frac{\partial J_{\mathrm{sum}}(\mathbf{w})}{\partial \mathbf{w}} = 4\mathbf{Q}_{\mathrm{sum}}(\mathbf{w}) \cdot \mathbf{w}} \tag{52}$$

with the (m,n)th element of $\mathbf{Q}_{\mathrm{sum}}(\mathbf{w})$ and $\partial^2 J_{\mathrm{sum}}(\mathbf{w})/\partial^2 \mathbf{w}$ equal to

$$\mathbf{Q}_{\mathrm{sum}}^{mn}(\mathbf{w}) = \sum_{i=1}^{M}\sum_{j=1}^{M} w(i)w(j)\rho_{ijmn}, \tag{53}$$

$$\frac{\partial^2 J_{\mathrm{sum}}(\mathbf{w})}{\partial w(m)\partial w(n)} = 4\sum_{i=1}^{M}\sum_{j=1}^{M} w(i)w(j)(2\rho_{ijmn} + \rho_{imjn}). \tag{54}$$

Hence, stationary points $\mathbf{w}_{\mathrm{s}}$, i.e. filter coefficients $\mathbf{w}$ for which the gradient $\partial J_{\mathrm{NL}}(\mathbf{w})/\partial \mathbf{w}$ is 0, satisfy

$$\boxed{(\mathbf{Q}_{\mathrm{sum}}(\mathbf{w}_{\mathrm{s}}) - \mathbf{Q}_{\mathrm{NL}})\mathbf{w}_{\mathrm{s}} = \mathbf{0}} \tag{55}$$

This implies that for a stationary point, either $\mathbf{w}_{\mathrm{s}} = \mathbf{0}$, or $\mathbf{Q}_{\mathrm{sum}}(\mathbf{w}_{\mathrm{s}}) = \mathbf{Q}_{\mathrm{NL}}$, or that $\mathbf{w}_{\mathrm{s}}$ lies in the null space of the matrix $\mathbf{Q}_{\mathrm{sum}}(\mathbf{w}_{\mathrm{s}}) - \mathbf{Q}_{\mathrm{NL}}$. Simulations indicate that several stationary points exist and that the latter condition is prevalent. In addition, it can be proved that the quadratic form $\mathbf{w}^{\mathrm{T}}\mathbf{H}_{\mathrm{NL}}(\mathbf{w})\mathbf{w}$ in a stationary point $\mathbf{w}_{\mathrm{s}}$ is equal to

$$\mathbf{w}_{\mathrm{s}}^{\mathrm{T}}\mathbf{H}_{\mathrm{NL}}(\mathbf{w}_{\mathrm{s}})\mathbf{w}_{\mathrm{s}} = 12\mathbf{w}_{\mathrm{s}}^{\mathrm{T}}\mathbf{Q}_{\mathrm{sum}}(\mathbf{w}_{\mathrm{s}})\mathbf{w}_{\mathrm{s}} - 4\mathbf{w}_{\mathrm{s}}^{\mathrm{T}}\mathbf{Q}_{\mathrm{NL}}\mathbf{w}_{\mathrm{s}} = 8\mathbf{w}_{\mathrm{s}}^{\mathrm{T}}\mathbf{Q}_{\mathrm{NL}}\mathbf{w}_{\mathrm{s}}. \tag{56}$$

Since in general the matrix $\mathbf{Q}_{\mathrm{NL}}$, defined in (41), is positive definite (only in very special cases $\mathbf{Q}_{\mathrm{NL}}$ is singular and hence positive semi-definite), the quadratic form $\mathbf{w}_{\mathrm{s}}^{\mathrm{T}}\mathbf{H}_{\mathrm{NL}}(\mathbf{w}_{\mathrm{s}})\mathbf{w}_{\mathrm{s}}$ is strictly positive in all stationary points except for $\mathbf{w}_{\mathrm{s}} = \mathbf{0}$, where it is equal to zero. Hence, *all stationary points are either local minima or saddle points*. For $\mathbf{w}_{\mathrm{s}} = \mathbf{0}$, the Hessian $\mathbf{H}_{\mathrm{NL}}(\mathbf{0}) = -4\mathbf{Q}_{\mathrm{NL}}$ is negative definite, such that $\mathbf{w}_{\mathrm{s}} = \mathbf{0}$ is the only local maximum.

Simulations have indicated that for each design problem a number of local minima exist, which are related to the symmetry present in the considered problem. For example, if $\mathbf{w}_m$ is a local minimum, then $-\mathbf{w}_m$ is a local minimum and for a symmetric linear array $\mathbf{J}_M\mathbf{w}_m$ also is a local minimum, with $\mathbf{J}_M$ the $M \times M$-dimensional reverse identity matrix. In these local minima the cost function has the same value, since (for a symmetric linear array)

$$d_{\mathrm{NL}} - \mathbf{w}_m^{\mathrm{T}}\mathbf{Q}_{\mathrm{NL}}\mathbf{w}_m = d_{\mathrm{NL}} - (-\mathbf{w}_m^{\mathrm{T}})\mathbf{Q}_{\mathrm{NL}}(-\mathbf{w}_m) = d_{\mathrm{NL}} - \mathbf{w}_m^{\mathrm{T}}\mathbf{J}_M\mathbf{Q}_{\mathrm{NL}}\mathbf{J}_M\mathbf{w}_m.$$

Simulations have also shown that other local minima exist, which appear not to be (easily) related to $\mathbf{w}_m$. However, the cost function in all local minima seems to be approximately equal, such that any of these local minima can be used as the final solution for the broadband beamformer.

3.5. Linear constraints

In this section several types of linear constraints are discussed, which can be imposed on the filter $\mathbf{w}$. These linear constraints can be written in the form

$$\mathbf{C}\mathbf{w} = \mathbf{b} \tag{57}$$

with $\mathbf{C}$ a $K \times M$-dimensional matrix (with the number of constraints $K \leqslant M$) and $\mathbf{b}$ a K-dimensional vector.

3.5.1. Point constraints

Point constraints can be used for constraining the spatial directivity pattern $H(\omega,\theta)$ to some predefined value at a specific frequency-angle point. The absolute point constraint $H(\omega_f,\theta_f) = b$, with $b = b_{\mathrm{R}} + jb_{\mathrm{I}}$ a complex scalar, corresponds to two real-valued constraints,

$$\begin{bmatrix} \mathbf{g}_{\mathrm{R}}^{\mathrm{T}}(\omega_f,\theta_f) \\ \mathbf{g}_{\mathrm{I}}^{\mathrm{T}}(\omega_f,\theta_f) \end{bmatrix} \mathbf{w} = \begin{bmatrix} b_{\mathrm{R}} \\ b_{\mathrm{I}} \end{bmatrix}, \tag{58}$$

whereas the relative point constraint $H(\omega_{f_1},\theta_{f_1}) = b\,H(\omega_{f_2},\theta_{f_2})$ can be written as

$$\begin{bmatrix} \mathbf{g}_{\mathrm{R}}^{\mathrm{T}}(\omega_{f_1},\theta_{f_1}) - b_{\mathrm{R}}\mathbf{g}_{\mathrm{R}}^{\mathrm{T}}(\omega_{f_2},\theta_{f_2}) + b_{\mathrm{I}}\mathbf{g}_{\mathrm{I}}^{\mathrm{T}}(\omega_{f_2},\theta_{f_2}) \\ \mathbf{g}_{\mathrm{I}}^{\mathrm{T}}(\omega_{f_1},\theta_{f_1}) - b_{\mathrm{I}}\mathbf{g}_{\mathrm{R}}^{\mathrm{T}}(\omega_{f_2},\theta_{f_2}) - b_{\mathrm{R}}\mathbf{g}_{\mathrm{I}}^{\mathrm{T}}(\omega_{f_2},\theta_{f_2}) \end{bmatrix} \mathbf{w} = \begin{bmatrix} 0 \\ 0 \end{bmatrix}. \tag{59}$$

3.5.2. Line constraint

Constraining $H(\omega,\theta)$ at the angle θ_f to a predefined frequency response $B(\omega) = \sum_{l=0}^{L-1} b_l \mathrm{e}^{-\mathrm{j}l\omega} = \mathbf{b}^{\mathrm{T}}\mathbf{e}(\omega)$, with $\mathbf{b}$ defined similarly as $\mathbf{w}_n$ in (3), corresponds to

$$H(\omega,\theta_f) = \sum_{n=0}^{N-1} W_n(\omega)\,\mathrm{e}^{-\mathrm{j}\omega\tau_n(\theta_f)} = \sum_{l=0}^{L-1} \left(\sum_{n=0}^{N-1} w_{n,l}\mathrm{e}^{-\mathrm{j}\omega\tau_n(\theta_f)} \right) \mathrm{e}^{-\mathrm{j}l\omega} \tag{60}$$

$$\triangleq B(\omega) = \sum_{l=0}^{L-1} b_l \mathrm{e}^{-\mathrm{j}l\omega}. \tag{61}$$

Obviously, this can be done by putting

$$\sum_{n=0}^{N-1} w_{n,l}\mathrm{e}^{-\mathrm{j}\omega\tau_n(\theta_f)} = b_l, \quad l = 0 \ldots L-1, \tag{62}$$

which corresponds to $2L$ real-valued constraints (assuming that the filter coefficients b_l are real), i.e.

$$\begin{bmatrix} \cos(\omega\tau_0(\theta_f))\mathbf{I}_L & \cos(\omega\tau_1(\theta_f))\mathbf{I}_L & \cdots & \cos(\omega\tau_{N-1}(\theta_f))\mathbf{I}_L \\ \sin(\omega\tau_0(\theta_f))\mathbf{I}_L & \sin(\omega\tau_1(\theta_f))\mathbf{I}_L & \cdots & \sin(\omega\tau_{N-1}(\theta_f))\mathbf{I}_L \end{bmatrix} \mathbf{w} = \begin{bmatrix} \mathbf{b} \\ \mathbf{0} \end{bmatrix}, \tag{63}$$

with $\mathbf{I}_L$ the $L \times L$-dimensional identity matrix. This equation has to hold *for all* ω. However, since $K = 2L \leqslant M$, in general these constraints can be satisfied maximally for $N/2$ frequency points. An exception exists for the angle $\theta_f = \pi/2$ (i.e. broadside direction), since in this case $\tau_n(\theta_f) = 0$, $n = 0 \ldots N-1$, such that (63) reduces to

$$[\mathbf{I}_L \;\; \mathbf{I}_L \;\; \cdots \;\; \mathbf{I}_L]\mathbf{w} = \mathbf{b}. \tag{64}$$

3.5.3. Derivative constraints

In order to smoothen $H(\omega,\theta)$, we can introduce derivative constraints, e.g. flattening the spatial directivity pattern at certain frequencies and angles by putting the frequency and/or angle derivatives to 0 [11], i.e.

$$\left.\frac{\partial H(\omega,\theta)}{\partial\theta}\right|_{\substack{\omega=\omega_f\\ \theta=\theta_f}} = 0, \qquad \left.\frac{\partial H(\omega,\theta)}{\partial\omega}\right|_{\substack{\omega=\omega_f\\ \theta=\theta_f}} = 0. \tag{65}$$

Since $H(\omega,\theta) = \mathbf{w}^{\mathrm{T}}\mathbf{g}(\omega,\theta)$, these derivatives are equal to

$$\frac{\partial H(\omega,\theta)}{\partial\theta} = \mathbf{w}^{\mathrm{T}}\underbrace{\frac{\partial \mathbf{g}(\omega,\theta)}{\partial\theta}}_{\mathbf{g}'_\theta(\omega,\theta)}, \qquad \frac{\partial H(\omega,\theta)}{\partial\omega} = \mathbf{w}^{\mathrm{T}}\underbrace{\frac{\partial \mathbf{g}(\omega,\theta)}{\partial\omega}}_{\mathbf{g}'_\omega(\omega,\theta)}. \tag{66}$$

Using (6), it can be shown that $\mathbf{g}'_\theta(\omega,\theta) = j\omega f_{\mathrm{s}}/c\sin\theta\boldsymbol{\Delta}_\theta\mathbf{g}(\omega,\theta)$, with $\boldsymbol{\Delta}_\theta$ an $M\times M$-dimensional diagonal matrix, containing the microphone distances,

$$\boldsymbol{\Delta}_\theta = \begin{bmatrix} d_0\mathbf{I}_L & & & \\ & d_1\mathbf{I}_L & & \\ & & \ddots & \\ & & & d_{N-1}\mathbf{I}_L \end{bmatrix}, \tag{67}$$

such that $\partial H(\omega,\theta)/\partial\theta|_{\substack{\omega=\omega_f\\ \theta=\theta_f}} = 0$ corresponds to two real-valued linear constraints,

$$\begin{bmatrix} \mathbf{g}_{\mathrm{R}}^{\mathrm{T}}(\omega_f,\theta_f) \\ \mathbf{g}_{\mathrm{I}}^{\mathrm{T}}(\omega_f,\theta_f) \end{bmatrix}\boldsymbol{\Delta}_\theta\mathbf{w} = \begin{bmatrix} 0 \\ 0 \end{bmatrix}. \tag{68}$$

4. Eigenfilter design procedures

In this section we present two novel non-iterative design procedures for broadband beamformers, which are based on eigenfilters. Eigenfilters have been introduced for designing one-dimensional linear phase FIR filters [34]. Their main advantage is the fact that no matrix inversion is required (as in LS filter design) and that time-domain and frequency-domain constraints are easily incorporated. Eigenfilter techniques have also been applied for designing two-dimensional FIR and spatial filters [4,29]. In this section, we extend the application domain of eigenfilters to the design of broadband beamformers.

In this section two eigenfilter-based cost functions will be considered:

- the conventional eigenfilter cost function J_{eig}, minimising the error between the spatial directivity patterns $D(\omega,\theta)H(\omega_c,\theta_c)/D(\omega_c,\theta_c)$ and $H(\omega,\theta)$. Note that a reference frequency-angle point (ω_c,θ_c) is required for this technique. Minimising this cost function with/without additional constraints leads to a (generalised) eigenvalue problem (cf. Section 4.1);
- the TLS eigenfilter cost function J_{TLS}, minimising the total least squares (TLS) error between the actual and the desired spatial directivity pattern. This cost function does not require a reference point and also leads to a generalised eigenvalue problem (cf. Section 4.2).

4.1. Conventional eigenfilter technique

4.1.1. General design

In the conventional eigenfilter technique a reference frequency-angle point (ω_c, θ_c) is chosen and the filter $\mathbf{w}$ is calculated such that the error between the spatial directivity patterns $H(\omega,\theta)$ and $D(\omega,\theta)H(\omega_c,\theta_c)/D(\omega_c,\theta_c)$ is minimised. Note that we do not specify the exact value of $H(\omega_c,\theta_c)$. The conventional eigenfilter cost function is defined as

$$J_{\text{eig}}(\mathbf{w}) = \int_{\Theta}\int_{\Omega} F(\omega,\theta)\left|\frac{D(\omega,\theta)}{D(\omega_c,\theta_c)}H(\omega_c,\theta_c) - H(\omega,\theta)\right|^2 \mathrm{d}\omega\,\mathrm{d}\theta. \tag{69}$$

Using (5) it can be shown that $J_{\text{eig}}(\mathbf{w})$ is equal to the quadratic form

$$\boxed{J_{\text{eig}}(\mathbf{w}) = \mathbf{w}^{\mathrm{T}}\mathbf{Q}_{\text{eig}}\mathbf{w}} \tag{70}$$

with $\mathbf{Q}_{\text{eig}}$ equal to

$$\int_{\Theta}\int_{\Omega} F(\omega,\theta)\,\mathrm{Re}\left\{\left[\frac{D(\omega,\theta)}{D(\omega_c,\theta_c)}\mathbf{g}(\omega_c,\theta_c) - \mathbf{g}(\omega,\theta)\right]\cdot\left[\frac{D(\omega,\theta)}{D(\omega_c,\theta_c)}\mathbf{g}(\omega_c,\theta_c) - \mathbf{g}(\omega,\theta)\right]^H\right\}\mathrm{d}\omega\,\mathrm{d}\theta. \tag{71}$$

When minimising the cost function $J_{\text{eig}}(\mathbf{w})$, an additional constraint is required in order to avoid the trivial solution $\mathbf{w} = \mathbf{0}$. Both a quadratic (energy) constraint and a linear constraint are possible and are discussed in Sections 4.1.3 and 4.1.4.

4.1.2. Specific design case

For the specific design case, assuming that the reference point (ω_c,θ_c) does not belong to the stopband region (Θ_s,Ω_s), the cost function $J_{\text{eig}}(\mathbf{w})$ in (69) can be written as

$$J_{\text{eig}}(\mathbf{w}) = \int_{\Theta_p}\int_{\Omega_p} |H(\omega_c,\theta_c) - H(\omega,\theta)|^2\,\mathrm{d}\omega\,\mathrm{d}\theta + \alpha\int_{\Theta_s}\int_{\Omega_s}|H(\omega,\theta)|^2\,\mathrm{d}\omega\,\mathrm{d}\theta, \tag{72}$$

such that the matrix $\mathbf{Q}_{\text{eig}}$ is equal to

$$\mathbf{Q}_{\text{eig}} = \underbrace{\int_{\Theta_p}\int_{\Omega_p}\mathrm{Re}\{[\mathbf{g}(\omega_c,\theta_c) - \mathbf{g}(\omega,\theta)][\mathbf{g}(\omega_c,\theta_c) - \mathbf{g}(\omega,\theta)]^H\}\,\mathrm{d}\omega\,\mathrm{d}\theta}_{\mathbf{Q}_p} + \alpha\underbrace{\int_{\Theta_s}\int_{\Omega_s}\mathbf{G}_R(\omega,\theta)\,\mathrm{d}\omega\,\mathrm{d}\theta}_{\mathbf{Q}_e^s}. \tag{73}$$

The quantity $\mathbf{w}^{\mathrm{T}}\mathbf{Q}_p\mathbf{w}$ is equal to the error in the passband, whereas $\mathbf{w}^{\mathrm{T}}\mathbf{Q}_e^s\mathbf{w}$ is equal to the energy (=error) in the stopband, such that

$$J_{\text{eig}}(\mathbf{w}) = \mathbf{w}^{\mathrm{T}}\underbrace{(\mathbf{Q}_p + \alpha\mathbf{Q}_e^s)}_{\mathbf{Q}_{\text{eig}}}\mathbf{w} \tag{74}$$

is a weighted error function over passband and stopband. The calculation of $\mathbf{Q}_e^s$ has been discussed in Section 3.2.2. If we define $\tilde{\mathbf{G}}(\omega_1,\theta_1,\omega_2,\theta_2)$ as

$$\tilde{\mathbf{G}}(\omega_1,\theta_1,\omega_2,\theta_2) = \mathbf{g}(\omega_1,\theta_1)\mathbf{g}^H(\omega_2,\theta_2), \tag{75}$$

then the expression $[\mathbf{g}(\omega_c,\theta_c)-\mathbf{g}(\omega,\theta)][\mathbf{g}(\omega_c,\theta_c)-\mathbf{g}(\omega,\theta)]^H$ can be written as

$$\hat{\mathbf{G}}(\omega,\theta,\omega_c,\theta_c)=\mathbf{G}(\omega_c,\theta_c)-\tilde{\mathbf{G}}(\omega,\theta,\omega_c,\theta_c)-\tilde{\mathbf{G}}(\omega_c,\theta_c,\omega,\theta)+\mathbf{G}(\omega,\theta), \tag{76}$$

which can be decomposed into a real and an imaginary part. Since the imaginary part $\hat{\mathbf{G}}_{\mathrm{I}}(\omega_c,\theta_c,\omega,\theta)$ is anti-symmetric, the integrand $|H(\omega_c,\theta_c)-H(\omega,\theta)|^2$ in (72) is equal to

$$|H(\omega_c,\theta_c)-H(\omega,\theta)|^2=\mathbf{w}^{\mathrm{T}}\hat{\mathbf{G}}_{\mathrm{R}}(\omega_c,\theta_c,\omega,\theta)\mathbf{w}, \tag{77}$$

such that the (i,j)th element of $\mathbf{Q}_{\mathrm{p}}$ is equal to

$$\mathbf{Q}_{\mathrm{p}}^{ij}=\int_{\Theta_{\mathrm{p}}}\int_{\Omega_{\mathrm{p}}}\hat{\mathbf{G}}_{\mathrm{R}}^{ij}(\omega_c,\theta_c,\omega,\theta)\,\mathrm{d}\omega\,\mathrm{d}\theta \tag{78}$$

$$\begin{aligned}
&=\int_{\Theta_{\mathrm{p}}}\int_{\Omega_{\mathrm{p}}}\cos\left[\omega_c\left((k-l)+\frac{(d_n-d_m)\cos\theta_c}{c}f_{\mathrm{s}}\right)\right]\mathrm{d}\omega\,\mathrm{d}\theta\\
&\quad-\int_{\Theta_{\mathrm{p}}}\int_{\Omega_{\mathrm{p}}}\cos\left[\omega\left(k+\frac{d_n\cos\theta}{c}f_{\mathrm{s}}\right)-\omega_c\left(l+\frac{d_m\cos\theta_c}{c}f_{\mathrm{s}}\right)\right]\mathrm{d}\omega\,\mathrm{d}\theta\\
&\quad-\int_{\Theta_{\mathrm{p}}}\int_{\Omega_{\mathrm{p}}}\cos\left[\omega\left(l+\frac{d_m\cos\theta}{c}f_{\mathrm{s}}\right)-\omega_c\left(k+\frac{d_n\cos\theta_c}{c}f_{\mathrm{s}}\right)\right]\mathrm{d}\omega\,\mathrm{d}\theta\\
&\quad+\int_{\Theta_{\mathrm{p}}}\int_{\Omega_{\mathrm{p}}}\cos\left[\omega_c\left((k-l)+\frac{(d_n-d_m)\cos\theta}{c}f_{\mathrm{s}}\right)\right]\mathrm{d}\omega\,\mathrm{d}\theta,
\end{aligned} \tag{79}$$

with $k=\mathrm{mod}(i-1,L)$, $l=\mathrm{mod}(j-1,L)$, $n=\lfloor(i-1)/L\rfloor$ and $m=\lfloor(j-1)/L\rfloor$. All these integrals can again be considered to be special cases of the integral

$$\int_{\theta_1}^{\theta_2}\int_{\omega_1}^{\omega_2}\cos[\omega(\alpha+\beta\cos\theta)+\gamma]\,\mathrm{d}\omega\,\mathrm{d}\theta, \tag{80}$$

of which the computation is discussed in Appendix A.

4.1.3. Quadratic energy constraint

The most common constraint on the filter $\mathbf{w}$ is the unit-norm (quadratic) constraint $\mathbf{w}^{\mathrm{T}}\mathbf{w}=1$, which leads to the following eigenvalue problem:

$$\min_{\mathbf{w}}\ \mathbf{w}^{\mathrm{T}}\mathbf{Q}_{\mathrm{eig}}\mathbf{w}\quad\text{subject to }\mathbf{w}^{\mathrm{T}}\mathbf{w}=1 \tag{81}$$

of which the solution is the eigenvector corresponding to the smallest eigenvalue of $\mathbf{Q}_{\mathrm{eig}}$ (hence the name eigenfilters).

In the one-dimensional FIR filter design case [34], this unit-norm constraint corresponds to the total area under the frequency response $|W(\omega)|^2$ being equal to 1, since using Parseval's theorem we can write

$$\int_0^{\pi}|W(\omega)|^2\frac{\mathrm{d}\omega}{\pi}=\mathbf{w}^{\mathrm{T}}\mathbf{w}. \tag{82}$$

In broadband beamformer design, a unit-norm constraint apparently does not have a physical meaning any more. Hence, we have modified this quadratic constraint by constraining the total area under the

spatial directivity spectrum $|H(\omega,\theta)|^2$ to be equal to 1, i.e.

$$\int_0^{\pi}\int_0^{\pi} |H(\omega,\theta)|^2 \,\mathrm{d}\omega\,\mathrm{d}\theta = \mathbf{w}^{\mathrm{T}}\mathbf{Q}_{\mathrm{e}}^{\mathrm{tot}}\mathbf{w} = \mathbf{1}, \tag{83}$$

with

$$\mathbf{Q}_{\mathrm{e}}^{\mathrm{tot}} = \int_0^{\pi}\int_0^{\pi} \mathbf{G}_{\mathrm{R}}(\omega,\theta)\,\mathrm{d}\omega\,\mathrm{d}\theta. \tag{84}$$

This constraint gives rise to the following constrained optimisation problem:

$$\boxed{\min_{\mathbf{w}} \mathbf{w}^{\mathrm{T}}\mathbf{Q}_{\mathrm{eig}}\mathbf{w} \quad \text{subject to } \mathbf{w}^{\mathrm{T}}\mathbf{Q}_{\mathrm{e}}^{\mathrm{tot}}\mathbf{w} = 1} \tag{85}$$

of which the solution $\mathbf{w}_{\mathrm{eig}}$ is the generalised eigenvector, corresponding to the minimum generalised eigenvalue in the GEVD of $\mathbf{Q}_{\mathrm{eig}}$ and $\mathbf{Q}_{\mathrm{e}}^{\mathrm{tot}}$.

4.1.4. Linear constraints

Instead of imposing a quadratic constraint, it is also possible to impose linear constraints $\mathbf{C}\mathbf{w} = \mathbf{b}$ in order to avoid the trivial solution $\mathbf{w} = \mathbf{0}$. We then have to solve the constrained optimisation problem

$$\min_{\mathbf{w}} \mathbf{w}^{\mathrm{T}}\mathbf{Q}_{\mathrm{eig}}\mathbf{w} \quad \text{subject to } \mathbf{C}\mathbf{w} = \mathbf{b}, \tag{86}$$

which is the same optimisation problem as (23) with $\mathbf{a} = \mathbf{0}$ and $d_{\mathrm{LS}} = 0$, such that solution (24) becomes

$$\mathbf{w}_{\mathrm{eig}}^{c} = \mathbf{Q}_{\mathrm{eig}}^{-1}\mathbf{C}^{\mathrm{T}}(\mathbf{C}\mathbf{Q}_{\mathrm{eig}}^{-1}\mathbf{C}^{\mathrm{T}})^{-1}\mathbf{b}. \tag{87}$$

4.2. Eigenfilter based on TLS error

4.2.1. General design

Recently, an eigenfilter based on a TLS error criterion has been described in [30] for designing two-dimensional FIR filters. The advantage of this eigenfilter is that no reference point is required. We have extended this TLS eigenfilter technique to the design of broadband beamformers. Instead of minimising the LS error (cf. Section 3.2), the TLS error

$$\frac{|D(\omega,\theta) - H(\omega,\theta)|^2}{\mathbf{w}^{\mathrm{T}}\mathbf{w} + 1} \tag{88}$$

is used and the cost function to be minimised can be written as

$$\bar{J}_{\mathrm{TLS}}(\mathbf{w}) = \int_{\Theta}\int_{\Omega} F(\omega,\theta)\frac{|D(\omega,\theta) - H(\omega,\theta)|^2}{\mathbf{w}^{\mathrm{T}}\mathbf{w} + 1}\,\mathrm{d}\omega\,\mathrm{d}\theta. \tag{89}$$

As in the conventional eigenfilter technique (cf. Section 4.1.3), we replace $\mathbf{w}^{\mathrm{T}}\mathbf{w}$ with $\mathbf{w}^{\mathrm{T}}\mathbf{Q}_{\mathrm{e}}^{\mathrm{tot}}\mathbf{w}$, which has a physical meaning, and instead minimise the cost function

$$J_{\mathrm{TLS}}(\mathbf{w}) = \int_{\Theta}\int_{\Omega} F(\omega,\theta)\frac{|D(\omega,\theta) - H(\omega,\theta)|^2}{\mathbf{w}^{\mathrm{T}}\mathbf{Q}_{\mathrm{e}}^{\mathrm{tot}}\mathbf{w} + 1}\,\mathrm{d}\omega\,\mathrm{d}\theta, \tag{90}$$

which can be written as

$$\boxed{J_{\mathrm{TLS}}(\mathbf{w}) = \frac{\hat{\mathbf{w}}^{\mathrm{T}}\hat{\mathbf{Q}}_{\mathrm{TLS}}\hat{\mathbf{w}}}{\hat{\mathbf{w}}^{\mathrm{T}}\hat{\mathbf{Q}}_{\mathrm{e}}^{\mathrm{tot}}\hat{\mathbf{w}}}} \tag{91}$$

with the extended vector $\hat{\mathbf{w}}$ and matrices $\hat{\mathbf{Q}}_{\mathrm{TLS}}$ and $\hat{\mathbf{Q}}_{\mathrm{e}}^{\mathrm{tot}}$ defined as

$$\hat{\mathbf{w}} = \begin{bmatrix} \mathbf{w} \\ -1 \end{bmatrix}, \quad \hat{\mathbf{Q}}_{\mathrm{TLS}} = \begin{bmatrix} \mathbf{Q}_{\mathrm{LS}} & \mathbf{a} \\ \mathbf{a}^{\mathrm{T}} & d_{\mathrm{LS}} \end{bmatrix}, \quad \hat{\mathbf{Q}}_{\mathrm{e}}^{\mathrm{tot}} = \begin{bmatrix} \mathbf{Q}_{\mathrm{e}}^{\mathrm{tot}} & \mathbf{0} \\ \mathbf{0}^{\mathrm{T}} & 1 \end{bmatrix}. \tag{92}$$

The definitions of $\mathbf{Q}_{\mathrm{LS}}$, $\mathbf{a}$ and d_{LS} are given in Sections 3.2.1 and 3.2.2, while the definition of $\mathbf{Q}_{\mathrm{e}}^{\mathrm{tot}}$ is given in Section 4.1.3. The filter $\hat{\mathbf{w}}_{\mathrm{TLS}}$ minimising $J_{\mathrm{TLS}}(\mathbf{w})$ is the generalised eigenvector of $\hat{\mathbf{Q}}_{\mathrm{TLS}}$ and $\hat{\mathbf{Q}}_{\mathrm{e}}^{\mathrm{tot}}$, corresponding to the smallest generalised eigenvalue. After scaling the last element of $\hat{\mathbf{w}}_{\mathrm{TLS}}$ to -1, the actual solution $\mathbf{w}_{\mathrm{TLS}}$ is obtained as the first M elements of $\hat{\mathbf{w}}_{\mathrm{TLS}}$.

4.2.2. Linear constraints

In [30] it is shown that linear constraints $\mathbf{C}\mathbf{w} = \mathbf{b}$ can be easily rewritten as

$$\hat{\mathbf{C}}\hat{\mathbf{w}} = \mathbf{0}, \quad \hat{\mathbf{C}} = [\mathbf{C} \quad \mathbf{b}], \tag{93}$$

such that the constrained optimisation problem can be rewritten as

$$\min_{\hat{\mathbf{w}}} \frac{\hat{\mathbf{w}}^{\mathrm{T}}\hat{\mathbf{Q}}_{\mathrm{TLS}}\hat{\mathbf{w}}}{\hat{\mathbf{w}}^{\mathrm{T}}\hat{\mathbf{Q}}_{\mathrm{e}}^{\mathrm{tot}}\hat{\mathbf{w}}} \quad \text{subject to } \hat{\mathbf{C}}\hat{\mathbf{w}} = \mathbf{0} \tag{94}$$

which is similar to (28) in Section 3.3.2. The solution $\tilde{\mathbf{w}}_{\mathrm{TLS}}$ of the unconstrained optimisation problem is given by the generalised eigenvector corresponding to the minimum generalised eigenvalue of $\mathbf{B}\hat{\mathbf{Q}}_{\mathrm{TLS}}\mathbf{B}^{\mathrm{T}}$ and $\mathbf{B}\hat{\mathbf{Q}}_{\mathrm{e}}^{\mathrm{tot}}\mathbf{B}^{\mathrm{T}}$ (with $\mathbf{B}$ the null space of $\hat{\mathbf{C}}$), such that the solution $\hat{\mathbf{w}}_{\mathrm{TLS}}^{c}$ of the constrained optimisation problem (94) is equal to

$$\hat{\mathbf{w}}_{\mathrm{TLS}}^{c} = \mathbf{B}^{\mathrm{T}}\tilde{\mathbf{w}}_{\mathrm{TLS}}. \tag{95}$$

After scaling the last element of $\hat{\mathbf{w}}_{\mathrm{TLS}}^{c}$ to -1, the actual solution $\mathbf{w}_{\mathrm{TLS}}^{c}$ is obtained as the first M elements of $\hat{\mathbf{w}}_{\mathrm{TLS}}^{c}$.

5. Near-field broadband beamformers

When the speech source is close to the microphone array, the far-field assumptions are no longer valid and spherical wavefronts (instead of planar wavefronts) and signal attenuation have to be taken into account. The typical rule of thumb is that the far-field assumptions are no longer valid when

$$r < \frac{d_{\mathrm{tot}}^2 f_{\mathrm{s}}}{c}, \tag{96}$$

with r the distance of the signal source to the centre of the microphone array, $d_{\mathrm{tot}} = d_{N-1} - d_0$ the total length of the (linear) microphone array, f_{s} the sampling frequency and c the speed of sound [26]. For example, for $d_{\mathrm{tot}} = 0.2$ m and $f_{\mathrm{s}} = 8$ kHz, the minimum distance for the far-field assumptions to be valid is $r = 0.94$ m. In this section it will be shown that *the design of near-field broadband beamformers is very similar to the design of far-field broadband beamformers* (*which are actually a special case for* $r \to \infty$). *All the cost functions from Sections 3 and 4 remain valid, whereas only the steering vector* $\mathbf{g}(\omega, \theta)$ *in* (6) *and all related quantities are defined differently for the near-field case.*

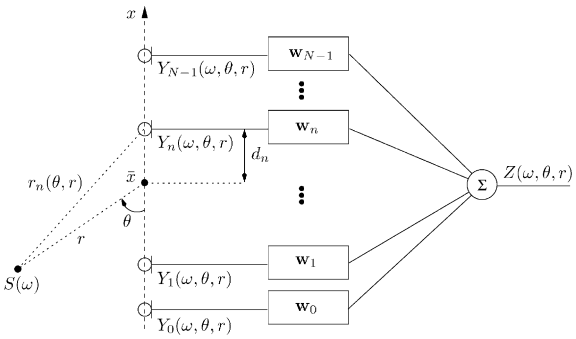

Fig. 2. Linear microphone array configuration (near-field).

5.1. Configuration

Consider the linear microphone array depicted in Fig. 2, where the speech source $S(\omega)$ is located at a distance r from the centre of the microphone array and with the angle θ as defined in the figure. Using simple geometrical relationships, the distance $r_n(\theta,r)$ from the source to the nth microphone is equal to

$$r_n(\theta,r)=\sqrt{(r\sin\theta)^2+(d_n+r\cos\theta)^2}=\sqrt{r^2+d_n^2+2d_n r\cos\theta}. \tag{97}$$

Taking into account spherical wavefronts and signal attenuation, the microphone signals $Y_n(\omega,\theta,r)$ are phase-shifted and attenuated versions of the signal $\bar{Y}(\omega,\theta,r)$ at the centre of the microphone array, $Y_n(\omega,\theta,r)=a_n(\theta,r)\mathrm{e}^{-\mathrm{j}\omega\tau_n(\theta,r)}\ \bar{Y}(\omega,\theta,r)$, with the attenuation $a_n(\theta,r)$ and the delay $\tau_n(\theta,r)$ equal to

$$\boxed{a_n(\theta,r)=\frac{r}{r_n(\theta,r)},\qquad \tau_n(\theta,r)=\frac{r_n(\theta,r)-r}{c}\,f_s}. \tag{98}$$

The spatial directivity pattern $H(\omega,\theta,r)$ is defined as

$$H(\omega,\theta,r)=\frac{Z(\omega,\theta,r)}{\bar{Y}(\omega,\theta,r)}=\frac{\sum_{n=0}^{N-1}W_n(\omega)Y_n(\omega,\theta,r)}{\bar{Y}(\omega,\theta,r)}. \tag{99}$$

Using (98), the spatial directivity pattern $H(\omega,\theta,r)$ can be written as

$$\boxed{H(\omega,\theta,r)=\sum_{n=0}^{N-1}a_n(\theta,r)W_n(\omega)\mathrm{e}^{-\mathrm{j}\omega\tau_n(\theta,r)}=\mathbf{w}^{\mathrm{T}}\mathbf{g}(\omega,\theta,r)} \tag{100}$$

with the M-dimensional steering vector $\mathbf{g}(\omega,\theta,r)$ now dependent of r,

$$\mathbf{g}(\omega,\theta,r)=\begin{bmatrix} a_0(\theta,r)\mathbf{e}(\omega)\mathrm{e}^{-\mathrm{j}\omega\tau_0(\theta,r)}\\ a_1(\theta,r)\mathbf{e}(\omega)\mathrm{e}^{-\mathrm{j}\omega\tau_1(\theta,r)}\\ \vdots\\ a_{N-1}(\theta,r)\mathbf{e}(\omega)\mathrm{e}^{-\mathrm{j}\omega\tau_{N-1}(\theta,r)}\end{bmatrix}. \tag{101}$$

As in the far-field case, the steering vector $\mathbf{g}(\omega,\theta,r)$ can be decomposed into a real part $\mathbf{g}_{\mathrm{R}}(\omega,\theta,r)$ and an imaginary part $\mathbf{g}_{I}(\omega,\theta,r)$. The ith element of the real part $\mathbf{g}_{R}(\omega,\theta,r)$ is equal to

$$\mathbf{g}_{\mathrm{R}}^{i}(\omega,\theta,r)=\frac{r\cos\left[\omega\left(k+\sqrt{(r^2+d_n^2+2d_n r\cos\theta}-r\right)f_{\mathrm{s}}/c\right)\right]}{\sqrt{r^2+d_n^2+2d_n r\cos\theta}},\quad i=1\ldots M, \tag{102}$$

with $k=\mathrm{mod}(i-1,L)$ and $n=[(i-1)/L]$. The spatial directivity spectrum $|H(\omega,\theta,r)|^2$ can be written as

$$|H(\omega,\theta,r)|^2=H(\omega,\theta,r)H^*(\omega,\theta,r)=\mathbf{w}^{\mathrm{T}}\mathbf{G}(\omega,\theta,r)\mathbf{w}, \tag{103}$$

with $\mathbf{G}(\omega,\theta,r)=\mathbf{g}(\omega,\theta,r)\mathbf{g}^{H}(\omega,\theta,r)$, which can also be decomposed into a real part $\mathbf{G}_{\mathrm{R}}(\omega,\theta,r)$ and an imaginary part $\mathbf{G}_{\mathrm{I}}(\omega,\theta,r)$. Since $\mathbf{G}_{\mathrm{I}}(\omega,\theta,r)$ is anti-symmetric, the spatial directivity spectrum $|H(\omega,\theta,r)|^2$ is equal to

$$\boxed{|H(\omega,\theta,r)|^2=\mathbf{w}^{\mathrm{T}}\mathbf{G}_{\mathrm{R}}(\omega,\theta,r)\mathbf{w}} \tag{104}$$

with the (i,j)th element of the real part $\mathbf{G}_{\mathrm{R}}(\omega,\theta,r)$ equal to

$$\mathbf{G}_{\mathrm{R}}^{ij}(\omega,\theta,r)=\frac{r^2\cos[\omega((k-l)+(r_n(\theta,r)-r_m(\theta,r))f_{\mathrm{s}}/c)]}{r_n(\theta,r)r_m(\theta,r)}. \tag{105}$$

The ultimate goal of broadband beamformer design is to design a beamformer such that the spatial directivity pattern $H(\omega,\theta,r)$ optimally fits a desired spatial directivity pattern $D(\omega,\theta,r)$ *for all distances* r, i.e.

$$\min_{\mathbf{w}}\int_R\int_\Theta\int_\Omega F(\omega,\theta,r)|H(\omega,\theta,r)-D(\omega,\theta,r)|^2\,\mathrm{d}\omega\,\mathrm{d}\theta\,\mathrm{d}r. \tag{106}$$

However, since this is quite a difficult task, near-field broadband beamformers are generally designed for one or a limited number of predefined distances, i.e. the outer integral in (106) is approximated by a finite sum.

5.2. Design for one distance

If the near-field broadband beamformer design is performed for *one fixed distance* r, the cost functions and derivations in Sections 3 and 4 remain valid, but the following substitutions have to be made:

$$H(\omega,\theta),\mathbf{g}(\omega,\theta),\mathbf{G}(\omega,\theta)\rightarrow H(\omega,\theta,r),\mathbf{g}(\omega,\theta,r),\mathbf{G}(\omega,\theta,r). \tag{107}$$

The only difference lies in the calculation of the double integrals. For details regarding this integral calculation, we refer to [7].

5.3. Mixed near-field far-field broadband beamforming

The spatial directivity pattern of a near-field broadband beamformer designed for one specific distance can be quite unsatisfactory at other distances (cf. simulations in Section 6). If the broadband beamformer should be able to operate at several distances—possibly having a different desired spatial directivity pattern $D(\omega,\theta,r)$ at these distances—we can define the total cost function

$$\boxed{J_{\mathrm{tot}}(\mathbf{w})=\sum_{r=1}^{R}\alpha_r J_r(\mathbf{w})} \tag{108}$$

with α_r a positive weighting factor, assigning more or less importance to the cost function $J_r(\mathbf{w})$. This cost function can be any of the cost functions from Sections 3 and 4, defined at distance r. If one of the considered distances is $r=\infty$, this is called mixed near-field far-field beamforming. For most design procedures (LS, non-linear criterion, conventional eigenfilter), this extension is straightforward. For example, in [37] mixed near-field far-field beamforming has been discussed for the LS cost function. However, for the TLS eigenfilter and the maximum energy array cost functions this extension gives rise to a significantly different optimisation problem, for which no closed-form solution is available.

5.3.1. TLS eigenfilter

The TLS eigenfilter cost function is equal to (cf. Section 4.2.1)

$$J_{\mathrm{TLS}}^{\mathrm{tot}}(\mathbf{w})=\sum_{r=1}^{R}\alpha_r J_{\mathrm{TLS},r}(\mathbf{w})=\sum_{r=1}^{R}\alpha_r\frac{\hat{\mathbf{w}}^{\mathrm{T}}\hat{\mathbf{Q}}_{\mathrm{TLS},r}\hat{\mathbf{w}}}{\hat{\mathbf{w}}^{\mathrm{T}}\hat{\mathbf{Q}}_{\mathrm{e},r}^{\mathrm{tot}}\hat{\mathbf{w}}}, \tag{109}$$

with

$$\hat{\mathbf{w}}=\begin{bmatrix}\mathbf{w}\\ -1\end{bmatrix},\quad \hat{\mathbf{Q}}_{\mathrm{TLS},r}=\begin{bmatrix}\mathbf{Q}_{\mathrm{LS},r} & \mathbf{a}_r\\ \mathbf{a}_r^{\mathrm{T}} & d_{\mathrm{LS},r}\end{bmatrix},\quad \hat{\mathbf{Q}}_{\mathrm{e},r}^{\mathrm{tot}}=\begin{bmatrix}\mathbf{Q}_{\mathrm{e},r}^{\mathrm{tot}} & \mathbf{0}\\ \mathbf{0}^T & 1\end{bmatrix}, \tag{110}$$

and $\hat{\mathbf{Q}}_{\mathrm{LS},r}$, $\mathbf{a}_r$, $d_{\mathrm{LS},r}$ and $\hat{\mathbf{Q}}_{\mathrm{e},r}^{\mathrm{tot}}$ defined at distance r.

The TLS eigenfilter cost function with linear constraints $\mathbf{C}\mathbf{w}=\mathbf{b}$ can be transformed into the unconstrained cost function (cf. Section 4.2.2)

$$\sum_{r=1}^{R}\alpha_r\frac{\tilde{\mathbf{w}}^{\mathrm{T}}\mathbf{B}\hat{\mathbf{Q}}_{\mathrm{TLS},r}\mathbf{B}^{\mathrm{T}}\tilde{\mathbf{w}}}{\tilde{\mathbf{w}}^{\mathrm{T}}\mathbf{B}\hat{\mathbf{Q}}_{\mathrm{e},r}^{\mathrm{tot}}\mathbf{B}^{\mathrm{T}}\tilde{\mathbf{w}}}. \tag{111}$$

Both minimising (109) and (111) can be considered to be special cases of minimising the cost function

$$\boxed{J_m(\mathbf{w})=\sum_{r=1}^{R}\frac{\mathbf{w}^{\mathrm{T}}\mathbf{A}_r\mathbf{w}}{\mathbf{w}^{\mathrm{T}}\mathbf{B}_r\mathbf{w}}} \tag{112}$$

with $\mathbf{A}_r$ and $\mathbf{B}_r$ symmetric positive-definite matrices. When $\mathbf{B}_r=\mathbf{B}$, $r=1\ldots R$, this problem is a generalised eigenvalue problem and the solution is given by the generalised eigenvector, corresponding to the minimum generalised eigenvalue of $\sum_{r=1}^{R}\mathbf{A}_r$ and $\mathbf{B}$. In general however, minimising $J_m(\mathbf{w})$ apparently cannot be transformed into a generalised eigenvalue problem. Hence, we have used an iterative non-linear optimisation technique for minimising this cost function. In order to improve the numerical robustness and the convergence speed of the optimisation technique, both the gradient

$$\frac{\partial J_m(\mathbf{w})}{\partial\mathbf{w}}=2\sum_{r=1}^{R}\frac{(\mathbf{w}^{\mathrm{T}}\mathbf{B}_r\mathbf{w})\mathbf{A}_r-(\mathbf{w}^{\mathrm{T}}\mathbf{A}_r\mathbf{w})\mathbf{B}_r}{(\mathbf{w}^{\mathrm{T}}\mathbf{B}_r\mathbf{w})^2}\,\mathbf{w} \tag{113}$$

and the Hessian

$$\begin{aligned}\frac{\partial^2 J_m(\mathbf{w})}{\partial^2\mathbf{w}}=&\,2\sum_{r=1}^{R}\frac{(\mathbf{w}^{\mathrm{T}}\mathbf{B}_r\mathbf{w})\mathbf{A}_r-(\mathbf{w}^{\mathrm{T}}\mathbf{A}_r\mathbf{w})\mathbf{B}_r+2(\mathbf{A}_r\mathbf{w}\mathbf{w}^{\mathrm{T}}\mathbf{B}_r-\mathbf{B}_r\mathbf{w}\mathbf{w}^{\mathrm{T}}\mathbf{A}_r)}{(\mathbf{w}^{\mathrm{T}}\mathbf{B}_r\mathbf{w})^2}\\ &-4\,\frac{[\mathbf{A}_r\mathbf{w}(\mathbf{w}^{\mathrm{T}}\mathbf{B}_r\mathbf{w})-\mathbf{B}_r\mathbf{w}(\mathbf{w}^{\mathrm{T}}\mathbf{A}_r\mathbf{w})]\mathbf{w}^{\mathrm{T}}\mathbf{B}_r}{(\mathbf{w}^{\mathrm{T}}\mathbf{B}_r\mathbf{w})^3}\end{aligned} \tag{114}$$

can be provided analytically. Although we have not been able to prove that this optimisation procedure converges to the global minimum, no problems with local minima have occurred during simulations.

5.3.2. Maximum energy array

The maximum energy array cost function is equal to (cf. Section 3.3.1)

$$J_{\mathrm{ME}}^{\mathrm{tot}}(\mathbf{w}) = \sum_{r=1}^{R} \alpha_r J_{\mathrm{ME},r}(\mathbf{w}) = \sum_{r=1}^{R} \alpha_r \frac{\mathbf{w}^{\mathrm{T}}\mathbf{Q}_{\mathrm{e},r}^{\mathrm{p}}\mathbf{w}}{\mathbf{w}^{\mathrm{T}}\mathbf{Q}_{\mathrm{e},r}^{\mathrm{s}}\mathbf{w}}, \tag{115}$$

with $\mathbf{Q}_{\mathrm{e},r}^{\mathrm{p}}$ and $\mathbf{Q}_{\mathrm{e},r}^{\mathrm{s}}$ defined at distance r. The maximum energy array cost function with linear constraints $\mathbf{C}\mathbf{w} = \mathbf{b}$ can be transformed into the unconstrained cost function (cf. Section 3.3.2)

$$\sum_{r=1}^{R} \alpha_r \frac{\tilde{\mathbf{w}}^{\mathrm{T}}\mathbf{B}\hat{\mathbf{Q}}_{\mathrm{e},r}^{\mathrm{p}}\mathbf{B}^{\mathrm{T}}\tilde{\mathbf{w}}}{\tilde{\mathbf{w}}^{\mathrm{T}}\mathbf{B}\hat{\mathbf{Q}}_{\mathrm{e},r}^{\mathrm{s}}\mathbf{B}^{\mathrm{T}}\tilde{\mathbf{w}}}. \tag{116}$$

Both maximising (115) and (116) can be considered to be a special case of maximising the cost function $J_m(\mathbf{w})$ in (112).

5.4. Linear constraints

Linear constraints of the form $\mathbf{C}\mathbf{w} = \mathbf{b}$ have been defined in Section 3.5 for the far-field case. For the near-field case, point constraints and derivative constraints can be defined similarly as for the far-field (for details we refer to [7]). However, a line constraint of the form (64) cannot be imposed for the near-field case, since for $\theta_f = \pi/2$ and $r \neq \infty$, the delays $\tau_n(\theta_f, r) \neq 0$.

6. Simulations

In this section, simulation results for far-field and near-field broadband beamformer design are discussed for the specific design case with $D(\omega,\theta) = 1$ in the passband and $D(\omega,\theta) = 0$ in the stopband. We have performed simulations using a linear uniform microphone array with $N = 5$ microphones, an inter-microphone distance $d = 4$ cm and sampling frequency $f_{\mathrm{s}} = 8$ kHz. Two specifications for the passband and the stopband have been considered:

- specification 1: passband $(\Omega_{\mathrm{p}}, \Theta_p) = (300\text{–}4000\ \mathrm{Hz},\ 70\text{–}110^\circ)$ and stopband $(\Omega_{\mathrm{s}}, \Theta_s) = (300\text{–}4000\ \mathrm{Hz},\ 0\text{–}60^\circ + 120\text{–}180^\circ)$
- specification 2: passband $(\Omega_{\mathrm{p}}, \Theta_{\mathrm{p}}) = (300\text{–}4000\ \mathrm{Hz},\ 40\text{–}80^\circ)$ and stopband $(\Omega_{\mathrm{s}}, \Theta_{\mathrm{s}}) = (300\text{–}4000\ \mathrm{Hz},\ 0\text{–}30^\circ + 90\text{–}180^\circ)$.

For the first specification, we have performed simulations without linear constraints and with a line constraint at 90°, whereas for the second specification, we have only performed simulations without linear constraints. For the conventional eigenfilter technique, the reference point for the first specification $(\omega_c, \theta_c) = (1500\ \mathrm{Hz}, 90^\circ)$ and for the second specification $(\omega_c, \theta_c) = (1500\ \mathrm{Hz}, 60^\circ)$. Both for the conventional eigenfilter technique and for the TLS eigenfilter technique, the matrix $\mathbf{Q}_{\mathrm{e}}^{\mathrm{tot}}$ is computed with frequency and angle specifications $(\Omega, \Theta) = (300\text{–}4000\ \mathrm{Hz},\ 0\text{–}180^\circ)$.

All broadband beamformers have been designed using the following parameters: filter length $L = 20$ and stopband weight $\alpha = 0.1, 1, 10$. For all beamformers we have computed the different cost functions[2] J_{LS}, J_{eig}, J_{TLS}, J_{ME} and J_{NL}, which have been defined in Sections 3 and 4. We will plot the total spatial directivity pattern $H(\omega,\theta)$ in the frequency-angle region $(\Omega, \Theta) = (300\text{–}3500\ \mathrm{Hz},\ 0\text{–}180^\circ)$ and the angular pattern for the specific frequencies $(500, 1000, 1500, 2000, 2500, 3500)$ Hz.

[2] Recall that the objective is to *minimise* J_{LS}, J_{eig}, J_{TLS} and J_{NL}, whereas the objective is to *maximise* J_{ME}.

Table 1
Different cost functions for design specification 1 without linear constraints

Design	α	J_{LS}	J_{eig}	J_{TLS}	J_{ME}	J_{NL}
LS	0.1	**0.07015**	0.02688	0.01803	3.87628	0.07734
EIG	0.1	0.08169	**0.02179**	0.02008	4.02636	0.06917
TLS	0.1	0.07234	0.02593	**0.01752**	3.51239	0.06759
ME	0.1	2824.61	0.92219	0.92061	**130.189**	$5.10\,10^7$
NL	0.1	0.63243	0.15624	0.14475	2.97090	**0.02540**
LS	1	**0.32012**	0.12644	0.10712	7.82490	0.24624
EIG	1	0.44332	**0.10786**	0.12097	10.9793	0.29769
TLS	1	0.34927	0.12651	**0.09851**	7.72356	0.18891
ME	1	2844.15	0.92856	0.92698	**130.189**	$5.10\,10^7$
NL	1	0.84110	0.24517	0.22330	5.24686	**0.10301**
LS	10	**1.00743**	0.58272	0.56422	17.83966	0.97683
EIG	10	2.10339	**0.44667**	0.51747	35.37774	2.52124
TLS	10	1.35343	0.54114	**0.44637**	22.22030	0.37251
ME	10	3039.51	0.99225	0.99065	**130.1890**	$5.10\,10^7$
NL	10	4.08658	1.61600	1.29464	18.66897	**0.21410**

6.1. Far-field design

Considering the *first design specification without linear constraints*, the different cost functions for the different beamformer design procedures are summarised in Table 1. Obviously, the design procedure optimising a specific cost function gives rise to the best value for this particular cost function (bold values). We will now compare the performance of the non-iterative design procedures (LS, EIG, TLS, ME) with the non-linear design procedure (NL) and determine which non-iterative design procedure has the best performance, using the non-linear cost function J_{NL} as a performance criterion. The maximum energy array technique has quite a poor performance (this can also be seen from the spatial directivity pattern in Fig. 6). In addition, the TLS eigenfilter technique always has a better performance than the LS technique (this is also true for other filter lengths and number of microphones). For small stopband weights α, the conventional eigenfilter technique also gives rise to a better performance than the LS technique, but this is not true any more for large stopband weights. Therefore, *the* TLS *eigenfilter technique appears to be the preferred non-iterative design procedure*, best resembling the performance of the non-linear design procedure but having a significantly lower computational complexity.

Figs. 3–7 show the spatial directivity patterns for all design procedures with $\alpha = 1$. Fig. 8 shows the spatial directivity pattern for the TLS eigenfilter technique with $\alpha = 10$.

When a *line constraint at* 90° is imposed, one can see by comparing Tables 1 and 2 that the cost functions with a line constraint are worse than the cost functions without constraint, but that all design procedures now give rise to quite similar results (also the maximum energy array technique). Again, the TLS eigenfilter technique has a better performance, i.e. non-linear cost function J_{NL}, than the LS, the maximum energy array and the conventional eigenfilter technique, such that it appears to be the preferred non-iterative design procedure. Fig. 9 shows the spatial directivity pattern for the TLS eigenfilter technique with $\alpha = 10$.

Considering the *second design specification without linear constraints*, the different cost functions for the different beamformer design procedures are summarised in Table 3 ($\alpha = 1$). Again, the maximum energy array technique has quite a poor performance. In addition, the TLS eigenfilter technique again has a better performance, i.e. non-linear cost function J_{NL}, than the LS, the maximum energy array and the conventional

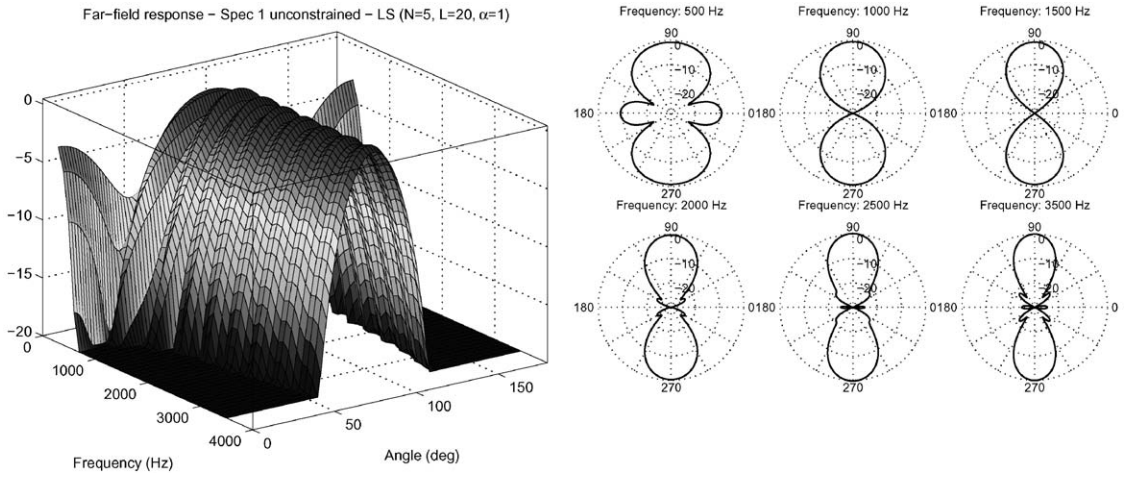

Fig. 3. LS technique (design specification 1, no linear constraints, $\alpha = 1$, $N = 5$, $L = 20$).

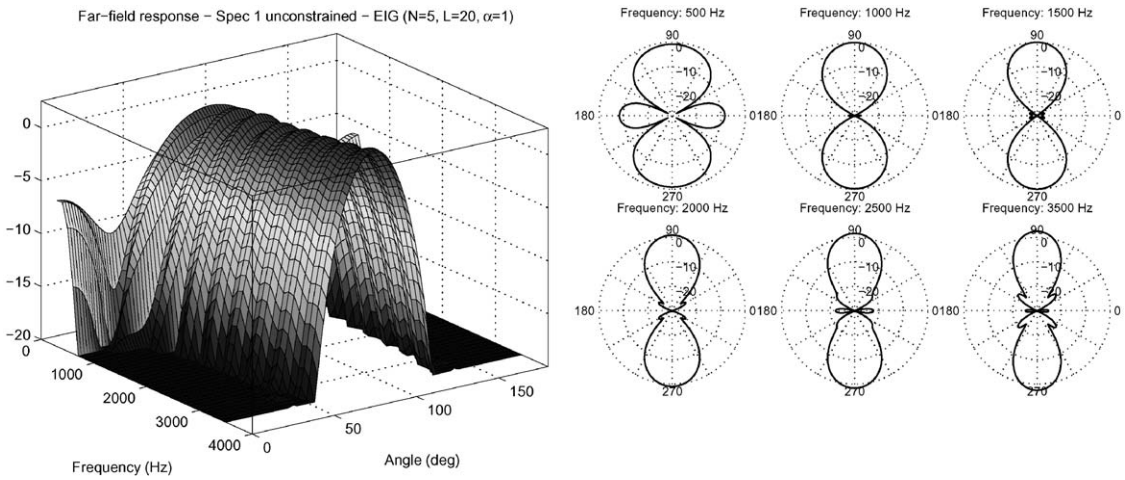

Fig. 4. Conventional eigenfilter technique (design specification 1, no linear constraints, $\alpha = 1$, $N = 5$, $L = 20$).

eigenfilter technique and therefore appears to be the preferred non-iterative design procedure. Figs. 10 and 11 show the spatial directivity patterns for the TLS eigenfilter technique and the non-linear criterion with $\alpha = 1$.

6.2. Mixed near-field far-field design

We have performed a mixed near-field far-field broadband beamformer design for $r = 0.2$ m (near-field) and $r = \infty$ (far-field) using the LS technique, the TLS eigenfilter technique and the non-linear criterion. The near-field weighting factor in (108) is $\alpha_r = 0.4$. We will only present results for the first design specification without linear constraints.

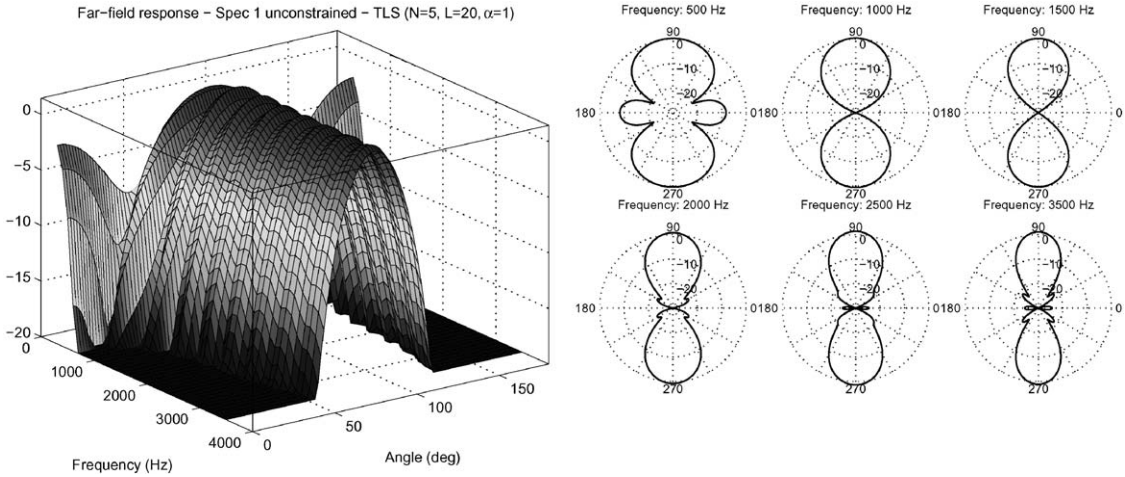

Fig. 5. TLS eigenfilter technique (design specification 1, no linear constraints, $\alpha = 1$, $N = 5$, $L = 20$).

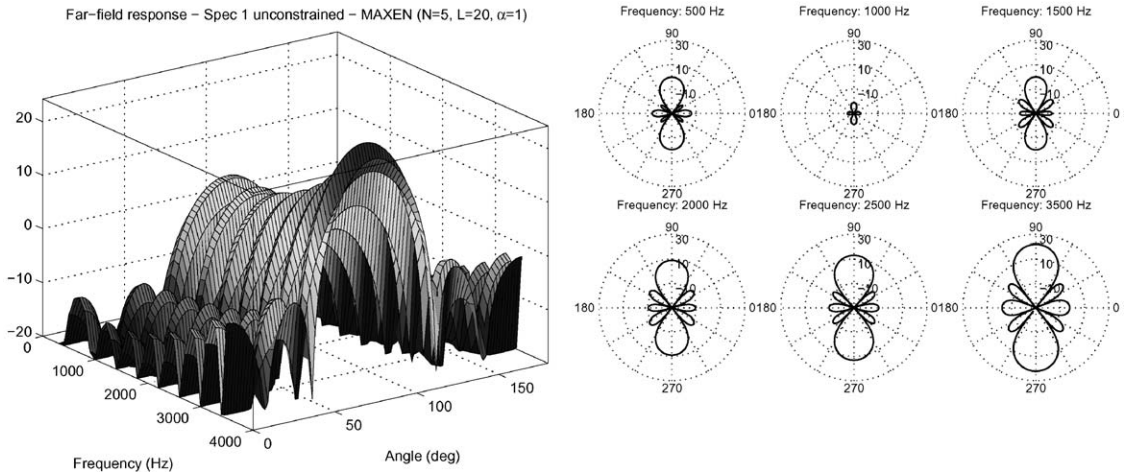

Fig. 6. Maximum energy array technique (design specification 1, no linear constraints, $\alpha = 1$, $N = 5$, $L = 20$).

Table 4 summarises the different cost functions (far-field, near-field, total) for the different design procedures (LS, TLS eigenfilter and non-linear design procedure for far-field, near-field and mixed near-field far-field) and for $\alpha = 1$. As can be seen, the far-field design yields the best far-field cost function, but gives rise to a poor near-field response. On the contrary, the near-field design yields the best near-field cost function, but gives rise to a poor far-field response. The mixed near-field far-field design provides a trade-off between the near-field and the far-field performance.

Fig. 12 shows the far-field and the near-field spatial directivity patterns for the TLS eigenfilter technique designed for the far-field (with $\alpha = 1$, $N = 5$, $L = 20$). As can be seen from this figure, the near-field response is quite unsatisfactory. Fig. 13 shows the far-field and the near-field spatial directivity patterns for the TLS eigenfilter technique designed for the near-field (with $\alpha = 1$, $N = 5$, $L = 20$). As can be seen from this figure, the far-field response now is quite unsatisfactory. Providing a trade-off between far-field and near-field

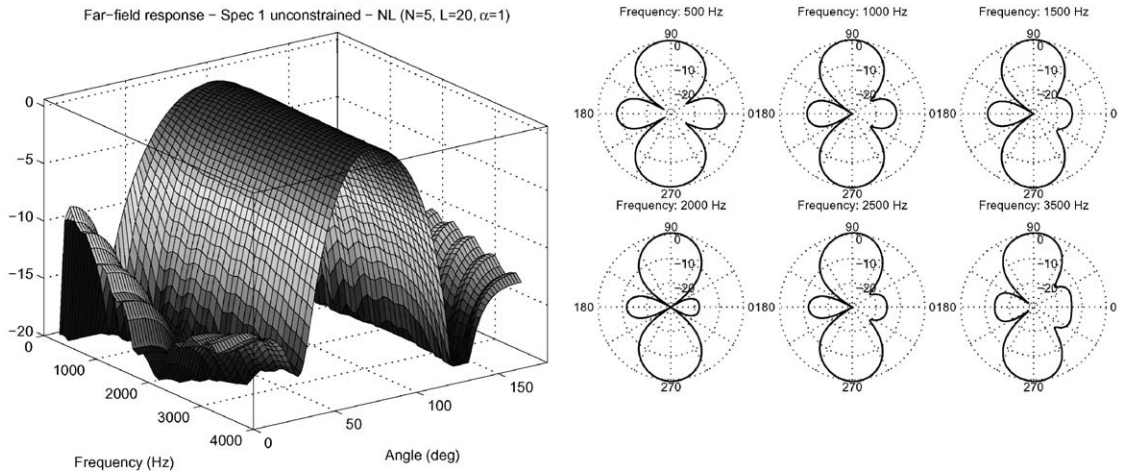

Fig. 7. Non-linear criterion (design specification 1, no linear constraints, $\alpha = 1$, $N = 5$, $L = 20$).

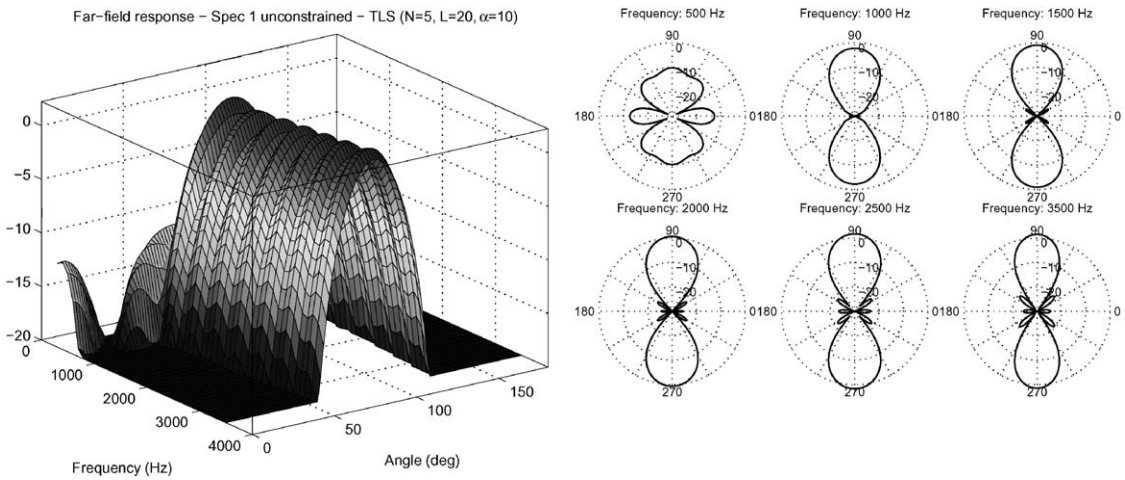

Fig. 8. TLS eigenfilter technique (design specification 1, no linear constraints, $\alpha = 10$, $N = 5$, $L = 20$).

Table 2
Different cost functions for design specification 1 with line constraint

Design	α	J_{LS}	J_{eig}	J_{TLS}	J_{ME}	J_{NL}
LS	10	**3.96204**	1.74435	1.21113	4.05166	1.85361
EIG	10	3.96204	**1.74435**	1.21113	4.05166	1.85361
TLS	10	3.99103	1.72361	**1.20375**	4.06720	1.83286
ME	10	3.97901	1.72672	1.20416	**4.06885**	1.84120
NL	10	5.01514	2.09900	1.47970	3.19583	**1.29136**

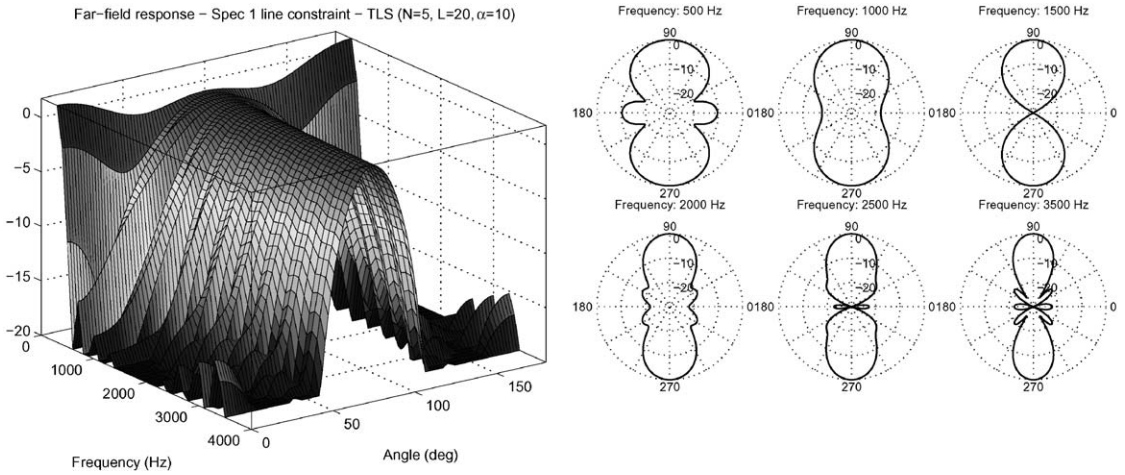

Fig. 9. TLS eigenfilter technique (design specification 1, line constraint, $\alpha = 10$, $N = 5$, $L = 20$).

Table 3
Different cost functions for design specification 2 without linear constraints

Design	α	J_{LS}	J_{eig}	J_{TLS}	J_{ME}	J_{NL}
LS	1	**0.50350**	0.24804	0.18191	4.62621	0.40657
EIG	1	3.54617	**0.15078**	0.94322	8.06733	0.29521
TLS	1	0.58258	0.24821	**0.15872**	4.58828	0.25312
ME	1	287.043	0.89290	0.87877	**38.9523**	252775
NL	1	1.98809	0.86805	0.54727	6.58217	**0.10891**

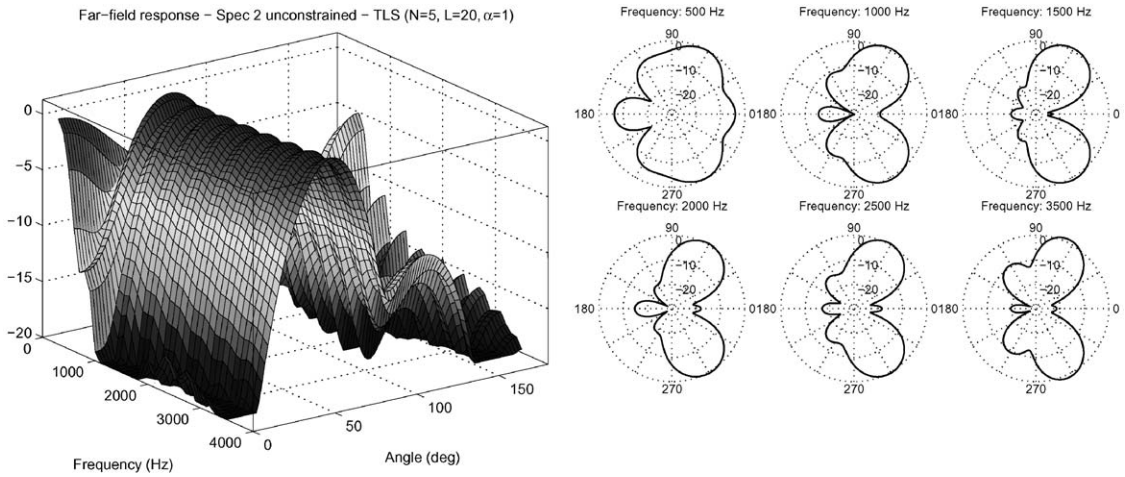

Fig. 10. TLS eigenfilter technique (design specification 2, no linear constraints, $\alpha = 1, N = 5$, $L = 20$).

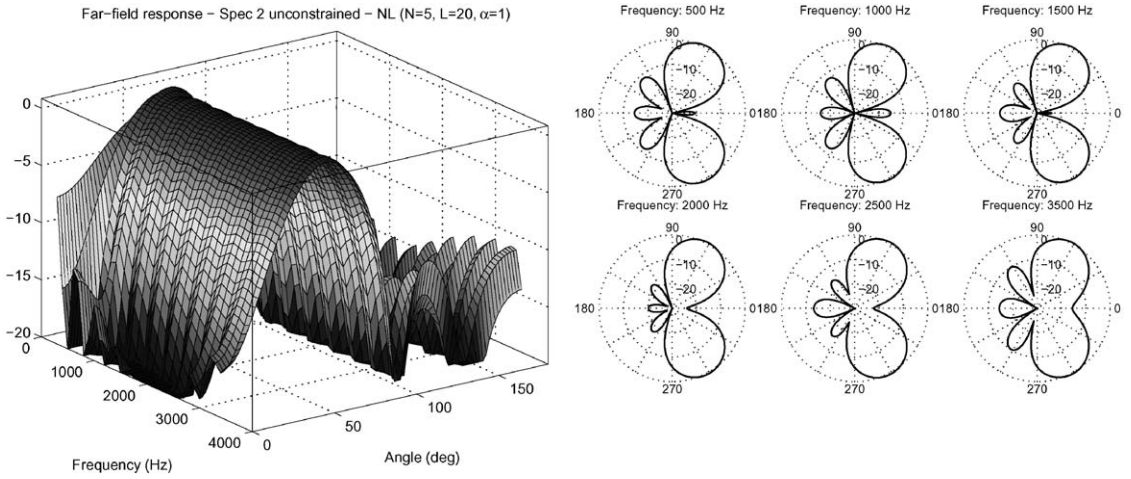

Fig. 11. Non-linear criterion (design specification 2, no linear constraints, $\alpha = 1$, $N = 5$, $L = 20$).

Table 4
Near-field, far-field and total cost function for different design procedures

Design	α	J_∞ (Far-field)	J_r (Near-field)	J_{tot} (Mixed)
LS Far-field	1	**0.32012**	1.68710	0.99496
LS Near-field	1	0.97135	**0.14284**	1.02849
LS Mixed	1	0.42277	0.45489	**0.60472**
TLS Far-field	1	**0.09851**	0.40205	0.25933
TLS Near-field	1	0.28515	**0.04309**	0.30239
TLS Mixed	1	0.12873	0.14564	**0.18698**
NL Far-field	1	**0.10301**	3.50694	1.50578
NL Near-field	1	0.45379	**0.08441**	0.48756
NL Mixed	1	0.15304	0.16557	**0.21926**

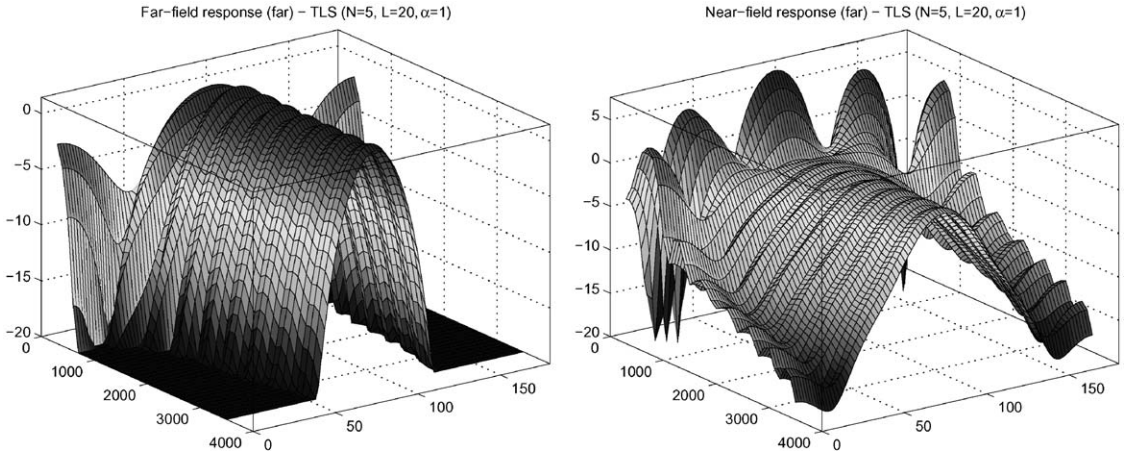

Fig. 12. Far-field and near-field spatial directivity pattern for TLS eigenfilter far-field design (design specification 1, $r = 0.2$ m, $\alpha = 1$, $N = 5$, $L = 20$).

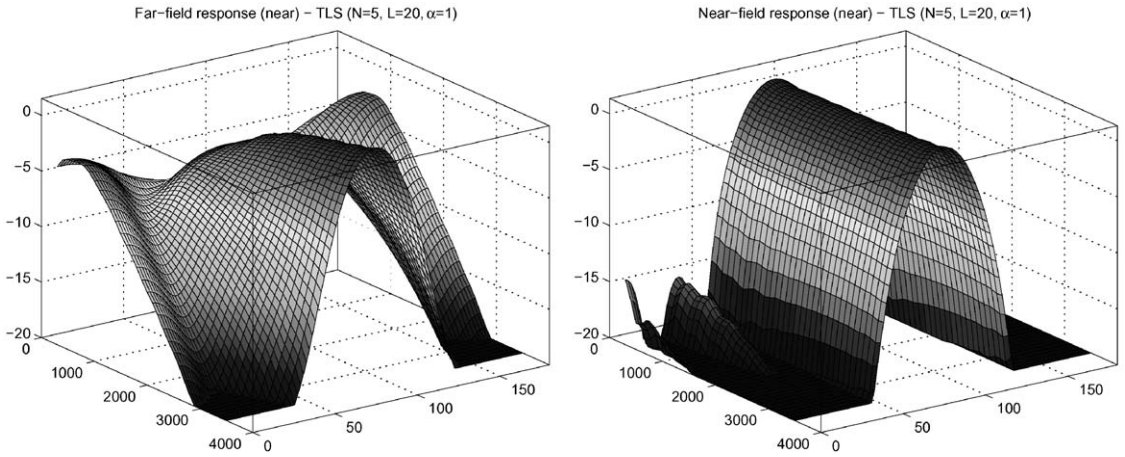

Fig. 13. Far-field and near-field spatial directivity pattern for TLS eigenfilter near-field design (design specification $1, r = 0.2$ m, $\alpha = 1$, $N = 5$, $L = 20$).

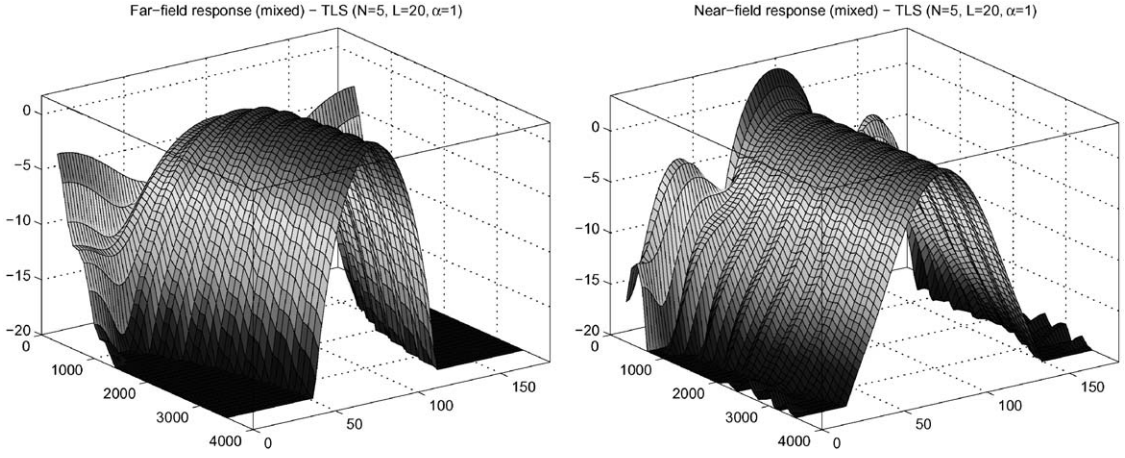

Fig. 14. Far-field and near-field spatial directivity pattern for TLS eigenfilter mixed near-field far-field design (design specification $1, r = 0.2$ m, $\alpha = 1$, $N = 5$, $L = 20$).

performance, Fig. 14 shows the far-field and the near-field spatial directivity patterns for the TLS eigenfilter technique that has been designed both for far-field and near-field (with $\alpha = 1$, $N = 5$, $L = 20$). Figs. 15–17 show similar results when the broadband beamformers are designed using the non-linear criterion.

7. Conclusion

In this paper we have described several design procedures for designing broadband beamformers with an arbitrary spatial directivity pattern using an arbitrary microphone configuration and an FIR filter-and-sum

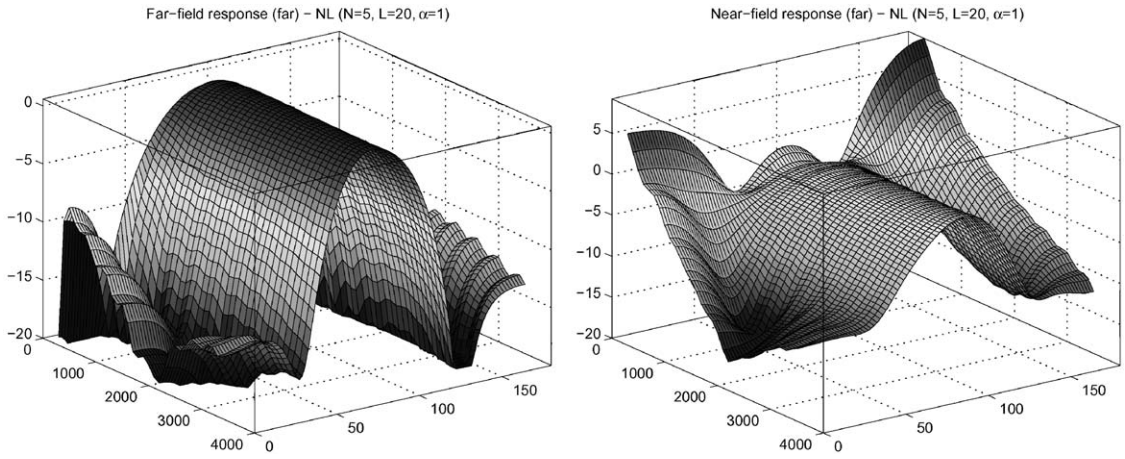

Fig. 15. Far-field and near-field spatial directivity pattern for non-linear far-field design (design specification $1, r = 0.2$ m, $\alpha = 1$, $N = 5$, $L = 20$).

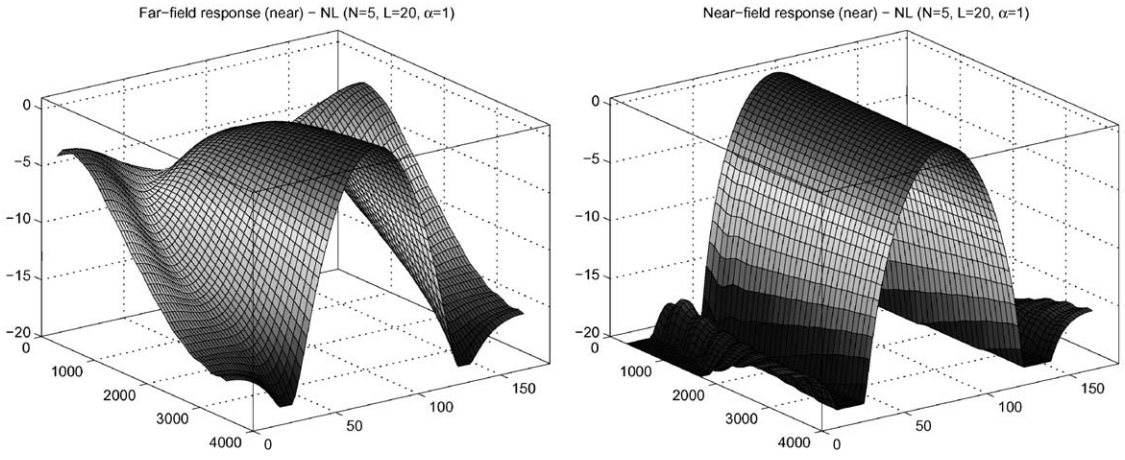

Fig. 16. Far-field and near-field spatial directivity pattern for non-linear near-field design (design specification $1, r = 0.2$ m, $\alpha = 1$, $N = 5$, $L = 20$).

structure. Several cost functions have been discussed: a LS cost function, a maximum energy array cost function, a non-linear criterion, and two novel non-iterative design procedures that are based on eigenfilters. In the conventional eigenfilter technique a reference frequency-angle point is required, whereas this reference point is not required in the TLS eigenfilter technique, minimising the TLS error between the actual and the desired spatial directivity pattern. We have shown that using these design procedures, broadband beamformers can be designed in the far-field, near-field and mixed near-field far-field. Different simulations have shown that among all considered non-iterative design procedures the TLS eigenfilter technique has the best performance, i.e. non-linear cost function J_{NL}, best resembling the performance of the non-linear design procedure but having a significantly lower computational complexity.

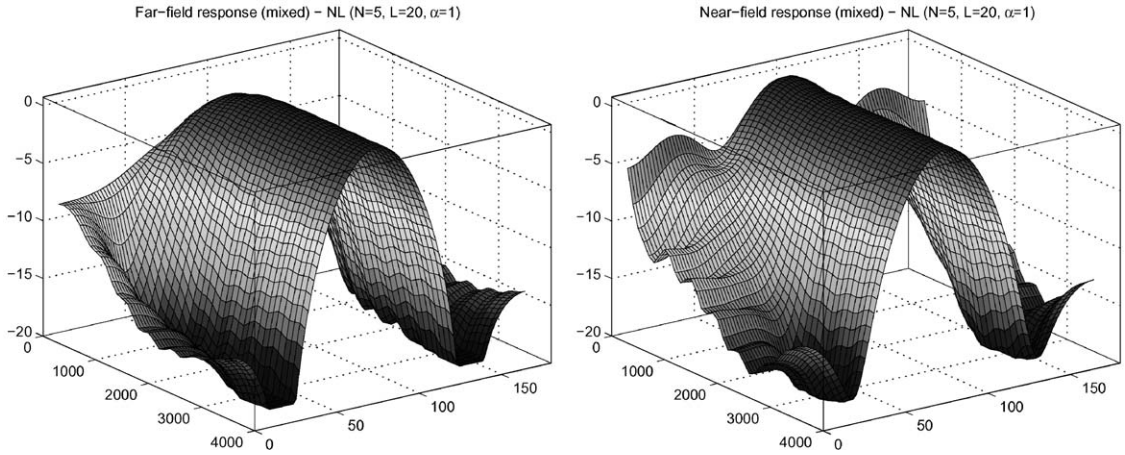

Fig. 17. Far-field and near-field spatial directivity pattern for non-linear mixed near-field far-field design (design specification $1, r = 0.2$ m, $\alpha = 1$, $N = 5$, $L = 20$).

Appendix A. Calculation of double integral for far-field design

The integral

$$I = \int_{\theta_1}^{\theta_2} \int_{\omega_1}^{\omega_2} \cos[\omega(\alpha + \beta\cos\theta) + \gamma]\,\mathrm{d}\omega\,\mathrm{d}\theta \tag{A.1}$$

is equal to

$$\int_{\theta_1}^{\theta_2} \frac{\sin[\omega_2(\alpha + \beta\cos\theta) + \gamma]}{\alpha + \beta\cos\theta}\,\mathrm{d}\theta - \int_{\theta_1}^{\theta_2} \frac{\sin[\omega_1(\alpha + \beta\cos\theta) + \gamma]}{\alpha + \beta\cos\theta}\,\mathrm{d}\theta, \tag{A.2}$$

such that in fact we need to compute integrals of the type (A.2),

$$I_\theta(\omega) = \int_{\theta_1}^{\theta_2} f(\omega, \theta)\,\mathrm{d}\theta, \tag{A.3}$$

with

$$\boxed{f(\omega, \theta) = \frac{\sin[\omega(\alpha + \beta\cos\theta) + \gamma]}{\alpha + \beta\cos\theta}}. \tag{A.4}$$

Normally, this integral can be computed numerically without any problem, but a special case occurs when $|\alpha| \leqslant |\beta|$, because then a singularity θ_n occurs in the denominator, with

$$\cos\theta_n = -\frac{\alpha}{\beta}, \tag{A.5}$$

such that numerically computing the integral $I_\theta(\omega)$ gives rise to numerical problems when $\gamma \neq 0$. By using the Taylor-expansion of $\cos\theta$ around θ_n, we can define the function $g(\theta)$,

$$g(\theta) = -\frac{\sin\gamma}{\beta\sqrt{1 - (\alpha^2/\beta^2)}(\theta - \theta_n)}, \tag{A.6}$$

which is a good approximation for $f(\omega,\theta)$ around θ_n and which is independent of ω. If we now define the function $\bar{f}(\omega,\theta) = f(\omega,\theta) - g(\theta)$, we can prove (by applying L'Hôpital's rule twice) that for any γ, $\lim_{\theta\to\theta_n} \bar{f}(\omega,\theta)$ is finite and is equal to

$$\lim_{\theta\to\theta_n} \bar{f}(\omega,\theta) = \omega\,\cos\gamma + \frac{\alpha\sin\gamma}{2(\alpha^2-\beta^2)}. \tag{A.7}$$

For details, we refer to [7]. Hence, the function $\bar{f}(\omega,\theta)$ can be integrated numerically without any problem. In fact, the total integral I in (A.1) can be written as

$$I = I_\theta(\omega_2) - I_\theta(\omega_1) = \int_{\theta_1}^{\theta_2} f(\omega_2,\theta)\,\mathrm{d}\theta - \int_{\theta_1}^{\theta_2} f(\omega_1,\theta)\,\mathrm{d}\theta \tag{A.8}$$

$$= \int_{\theta_1}^{\theta_2} \bar{f}(\omega_2,\theta)\,\mathrm{d}\theta - \int_{\theta_1}^{\theta_2} \bar{f}(\omega_1,\theta)\,\mathrm{d}\theta. \tag{A.9}$$

References

[1] Acoustical Society of America, ANSI S3.5-1997, American National Standard Methods for Calculation of the Speech Intelligibility Index, June 1997.

[2] J. Bitzer, K.U. Simmer, Superdirective microphone arrays, in: M.S. Brandstein, D.B. Ward (Eds.), Microphone Arrays: Signal Processing Techniques and Applications, Springer, Berlin, 2001, pp. 19–38 (Chapter 2).

[3] K.M. Buckley, Broad-band beamforming and the generalized sidelobe canceller, IEEE Trans. Acoust. Speech Signal Process. 34 (5) (1986) 1322–1323.

[4] T. Chen, Unified eigenfilter approach: with applications to spectral/spatial filtering, in: Proceedings of the IEEE International Symposium on Circuits and Systems (ISCAS), Chicago, USA, 1993, pp. 331–334.

[5] T. Coleman, M.A. Branch, A. Grace, MATLAB Optimization Toolbox User's Guide, The Mathworks, Inc., Natick, MA, USA, 1999.

[6] H. Cox, R. Zeskind, T. Kooij, Practical supergain, IEEE Trans. Acoust. Speech Signal Process. 34 (3) (1986) 393–398.

[7] S. Doclo, Multi-microphone noise reduction and dereverberation techniques for speech applications, Ph.D. Thesis, ESAT, Katholieke Universiteit Leuven, Belgium, May 2003.

[8] C.L. Dolph, A current distribution for broadside arrays which optimizes the relationship between beam width and sidelobe level, Proc. IRE 34 (1946) 335–348.

[9] G.W. Elko, Microphone array systems for hands-free telecommunication, Speech Commun. 20 (3–4) (1996) 229–240.

[10] G. Elko, Superdirectional microphone arrays, in: S.L. Gay, J. Benesty (Eds.), Acoustic Signal Processing for Telecommunication, Kluwer Academic Publishers, Dordrecht, Boston, 2000, pp. 181–237 (Chapter 10).

[11] M.H. Er, A. Cantoni, Derivative constraints for broad-band element space antenna array processors, IEEE Trans. Acoust. Speech Signal Process. 31 (6) (1983) 1378–1393.

[12] R. Fletcher, Practical Methods of Optimization, Wiley, New York, 1987.

[13] O.L. Frost III, An algorithm for linearly constrained adaptive array processing, Proc. IEEE 60 (1972) 926–935.

[14] J.E. Greenberg, P.M. Zurek, Microphone-array hearing aids, in: M.S. Brandstein, D.B. Ward (Eds.), Microphone Arrays: Signal Processing Techniques and Applications, Springer, Berlin, 2001, pp. 229–253 (Chapter 11).

[15] L.J. Griffiths, C.W. Jim, An alternative approach to linearly constrained adaptive beamforming, IEEE Trans. Antennas Propagat. 30 (1982) 27–34.

[16] O. Hoshuyama, A. Sugiyama, A. Hirano, A robust adaptive beamformer for microphone arrays with a blocking matrix using constrained adaptive filters, IEEE Trans. Signal Process. 47 (10) (1999) 2677–2684.

[17] M. Kajala, M. Hämäläinen, Broadband beamforming optimization for speech enhancement in noisy environments, in: Proceedings of the IEEE Workshop on Applications of Signal Processing to Audio and Acoustics (WASPAA), New Paltz, NY, USA, 1999, pp. 19–22.

[18] J.M. Kates, Superdirective arrays for hearing aids, J. Acoust. Soc. Am. 94 (4) (1993) 1930–1933.

[19] J.M. Kates, M.R. Weiss, A comparison of hearing-aid array-processing techniques, J. Acoust. Soc. Am. 99 (5) (1996) 3138–3148.

[20] W. Kellermann, A self-steering digital microphone array, in: Proceedings of the IEEE International Conference on Acoustics, Speech, and Signal Processing (ICASSP), Toronto, Canada, 1991, pp. 3581–3584.
[21] R.A. Kennedy, T. Abhayapala, D.B. Ward, R.C. Williamson, Nearfield broadband frequency invariant beamforming, in: Proceedings of the IEEE International Conference on Acoustics, Speech, and Signal Processing (ICASSP), Atlanta GA, USA, 1996, pp. 905–908.
[22] D. Korompis, K. Yao, F. Lorenzelli, Broadband maximum energy array with user imposed spatial and frequency constraints, in: Proceedings of the IEEE International Conference on Acoustics, Speech, and Signal Processing (ICASSP), Adelaide, Australia, 1994, pp. 529–532.
[23] B.K. Lau, Y.H. Leung, K.L. Teo, V. Sreeram, Minimax filters for microphone arrays, IEEE Trans. Circuits Systems II 46 (12) (1999) 1522–1525.
[24] H. Lebret, S. Boyd, Antenna array pattern synthesis via convex optimization, IEEE Trans. Signal Process. 45 (3) (1997) 526–532.
[25] W.-S. Lu, A. Antoniou, Design of digital filters and filter banks by optimization: a state of the art review, in: Proceedings of the European Signal Processing Conference (EUSIPCO), Tampere, Finland, 2000, pp. 351–354.
[26] R.J. Mailloux, Phased Array Antenna Handbook, Artech House, Boston, 1994.
[27] S. Nordebo, I. Claesson, S. Nordholm, Weighted Chebyshev approximation for the design of broadband beamformers using quadratic programming, IEEE Signal Process. Lett. 1 (7) (1994) 103–105.
[28] S. Nordebo, I. Claesson, S. Nordholm, Adaptive beamforming: spatial filter designed blocking matrix, IEEE J. Oceanic Eng. 19 (4) (1994) 583–590.
[29] S.-C. Pei, J.-J. Shyu, 2-D FIR eigenfilters: a least-squares approach, IEEE Trans. Circuits Systems 37 (1) (1990) 24–34.
[30] S.-C. Pei, C.-C. Tseng, A new eigenfilter based on total least squares error criterion, IEEE Trans. Circuits Systems I 48 (6) (2001) 699–709.
[31] J.G. Ryan, R.A. Goubran, Array optimization applied in the near field of a microphone array, IEEE Trans. Speech Audio Process. 8 (2) (2000) 173–176.
[32] W. Soede, A.J. Berkhout, F.A. Bilsen, Development of a directional hearing instrument based on array technology, J. Acoust. Soc. Am. 94 (2) (1993) 785–798.
[33] R.W. Stadler, W.M. Rabinowitz, On the potential of fixed arrays for hearing aids, J. Acoust. Soc. Am. 94 (3) (1993) 1332–1342.
[34] P.P. Vaidyanathan, T.Q. Nguyen, Eigenfilters: a new approach to least-squares FIR filter design and applications including Nyquist filters, IEEE Trans. Circuits Systems 34 (1) (1987) 11–23.
[35] S. Van Gerven, D. Van Compernolle, P. Wauters, W. Verstraeten, K. Eneman, K. Delaet, Multiple beam broadband beamforming: filter design and real-time implementation, in: Proceedings of the IEEE Workshop on Applications of Signal Processing to Audio and Acoustics (WASPAA), New Paltz, NY, USA, 1995, pp. 173–176.
[36] B.D. Van Veen, K.M. Buckley, Beamforming: a versatile approach to spatial filtering, IEEE ASSP Mag. 5 (2) (1988) 4–24.
[37] D.B. Ward, G.W. Elko, Mixed nearfield/farfield beamforming: a new technique for speech acquisition in a reverberant environment, in: Proceedings of the IEEE Workshop on Applications of Signal Processing to Audio and Acoustics (WASPAA), New Paltz, NY, USA, 1997.
[38] D.B. Ward, R.A. Kennedy, R.C. Williamson, Theory and design of broadband sensor arrays with frequency invariant far-field beam patterns, J. Acoust. Soc. Am. 97 (2) (1995) 91–95.
[39] D.B. Ward, R.A. Kennedy, R.C. Williamson, Constant directivity beamforming, in: M.S. Brandstein, D.B. Ward (Eds.), Microphone Arrays: Signal Processing Techniques and Applications, Springer, Berlin, 2001, pp. 3–17 (Chapter 1).